ICE-SHEET INTERACTION WITH A CABLE-MOORED PLATFORM

by

Wilfrid A. Nixon and Robert Ettema

Submitted to

Hitachi Zosen Corporation, Osaka, Japan
Mobil Research and Development Corporation, Dallas, Texas
Minerals Management Service, Washington, D.C.

IIHR Limited Distribution Report No.

Iowa Institute of Hydraulic Research
The University of Iowa
Iowa City, Iowa 52242-1585

December 1987

TABLE OF CONTENTS

ABSTRACT

Fourty-two tests of a model cable moored platform have been conducted in IIHR ice towing tank facility. In each test, a sheet of urea doped ice, with thickness from 20-40mm and bending strength between 25 and 40kPa, was driven past the model platform. The platform was tested in two modes: "Fixed", in which no deflection of the platform was allowed, and "moored", in which the platform could surge, heave and pitch against restoring forces provided by buoyancy (for heave and pitch) and a leaf spring (for surge).

The observed behavior indicated that, for both moored and fixed platform geometries, the forces on the plataform increased with increasing ice thickness. The fixed plataform experienced increasing forces as the ice impact velocity increased but for the moored platform any such response was masked by resonance effects. The critical frequency in this regard was the breaking frequency of the ice for the heave and pitch forces on the moored platform. However, the surge force power spectrum was dominated by the natural frequency of the platform.

A most interesting result of the study is that the mooring forces on the plataform appear to experience a minimum with respect to the stiffness of the mooring system. Such a result has obvious practical implications, and will be investigated further.

ACKNOWLEDGEMENTS

The authors wish to thank Dr. M. Matsuishi of Hitachi Zosen Corporation, Dr. R. Johnson of Mobil Research and Development Corporation and Mr. C. Smith of U.S. Minerals Management Service for their guidance in conduct of this project. Additionally, the authors wish to thank Mr. S. Iwata of Hitachi Zosen Corporation for assisting in conduct of the experiment.

LIST OF FIGURES

LIST OF TABLES

I. INTRODUCTION

Drilling for oil in relatively deep, ice-covered or ice-infested waters poses a number of problems, not least of which is the provision of a stable platform from which drilling activities can be conducted. A cable-moored platform of conical hull shape provides such stability, and experience with one platform, "Kulluk," (see e.g., Hnatiuk and Wright, 1984) in the Beaufort Sea. Figure 1 shows the hull shape and mooring configuration of a model floating, conical platform similar to "Kulluk." This model was used in all the experiments described herein.

While "Kulluk" operated with success in the Beaufort Sea, there remain to be answered a number of concerns for the designers and operators of such floating platforms. Obviously of importance are the forces, displacements and accelerations (the dynamic response) of the platform as it encounters a variety of different ice types (ice sheets, ice floe fields, rubble ice, large individual floes, etc.). Knowledge of the dynamic response "envelope" of a platform will enable decisions regarding emergency movement of the platform (due to unacceptable ice conditions) to be made more effectively, avoiding unnecessary "downtime" and also unsafe operations. Another area of concern is the problem caused by ice underriding the platform, and potentially damaging the drill string. Indeed, this latter event may be a more important factor in determining safe operation than the ice forces. Also of importance is the effect of mooring system stiffness on the dynamic response of a platform. This may even allow some "tuning" of platform dynamic response to be made according to prevailing ice condition.

A. Scope of Study

The principle objectives of the study were to determine the effects of mooring system stiffness, ice sheet thickness, ice sheet strength and ice sheet velocities on the forces and motions (accelerations and displacements) that a conical platform would encounter while amidst a large, moving ice sheet.

To meet these objectives, model tests were conducted at IIHR's ice towing tank, using a 1.5-meter-diameter (at the load waterline) test platform. The model platform, shown in figure 2, was approximately a 1:45-scale replica of

the hull of the existing platform "Kulluk." However, it did not exactly replicate "Kulluk", as it was somewhat simpler in hull form and "Kulluk's" mooring system was not simulated exactly.

The ice sheets were grown and tempered to the required thicknesses and strengths by means of the methods described below. After tempering, the sheets were pushed against the platform by the tank carriage.

The results obtained from the tests are compared with the performance criteria for the cable mooring system of the platform "Kulluk."

B. Practical Aspects

A cable-moored platform of the type shown in figure 1 is obviously only one of a number of design concepts under consideration for operation in ice covered waters. No single platform is ideal for all Arctic drilling sites, and the most suitable platform type is determined by, typically, the water depth and the ice conditions at the drilling sites. Frederking (1984) reviews the various platform concepts.

Cable-moored platforms appear best suited to water depths between 20-60 meters. "Kulluk" was designed to withstand ice floes of 1 to 1.5m thickness of annual ice. In worse ice conditions, it is to be towed from the drill site. Additional protection was to be provided by ice-breaking ships acting as escort (Huatink and Wright, 1984; Loh and Stamberg, 1984).

C. Previous Work

A detailed review of previous work, both practical and theoretical, concerning ice forces against inclined planes and conical structures is given by Matsuishi and Ettema (1985a). The interested reader is referred to this report.

Relatively few tests have been performed on models of cable-moored structures. Frederking and Schwarz (1982) conducted a series of tests investigating the ice-breaking performance of a downward breaking cone. For some tests, the cone was restrained from moving, while in other tests, it was allowed to oscillate both vertically and horizontally. The oscillating cone experienced a horizontal force only two-thirds of that measured for the restrained cone.

Matsuishi and Ettema (1985a,b) conducted tests on the model platform used in the present study to investigate the dynamic behavior of the platform when impacted by floes of annual ice, and when in a field of mushy ice. They made measurements both with the platform fixed and with it "moored." As in this series of tests, mooring system stiffness was modelled using a leaf spring (see Section II, below). Among the results they obtained were:

1. That mooring force, platform motions and accelerations increased with increasing floe diameter, but asymptotically approached a constant value when floe diameter exceeding platform waterline diameter.
2. That mooring forces increased with increasing speed of ice floe impact.
3. That when impacted by mushy ice, the moored platform experienced a force that increased monotonically as a "prow" developed around the leading edge of the platform. Once the "prow" had reached an equilibrium size, the ice loads remained steady.
4. In mushy ice, the mooring forces were linearly proportional to the thickness of the ice rubble layer.

It is intended that this study should build on the work of Matsuishi and Ettema (1985a,b).

II. EXPERIMENTAL PROCEDURE

A. Test Facilities

1. IIHR's ice towing tank.

All experiments were conducted using IIHR's ice towing tank which is 20m long, 5m wide and 1.3m deep. Figure 3 shows the layout of the tank, and cold room within which it is housed. Depending on the external ambient temperature, the cold room has a cooling capacity between 15 and 20kw, allowing an ice sheet to grow at a rate of 1.5 to 2.0mm per hour.

A motorized carriage (shown in figure 4) was used to push the ice sheets against the model platform. The carriage is driven by a variable velocity D.C. motor, and can move at velocities between 0.001 to 1.50m/s. Velocity is accurately measured by means of a wheel carrying a circular array of regularly

spaced holes, which is mounted on the drive shaft of the motor. A light shines on one side of the wheel and, as a hole passes, the light is detected on the other side of the wheel by a photo detector. The number of "pulses" detected per second is linearly proportional to the carriage velocity.

2. The test platform.

The test platform is similar, but not exactly identical, in form to the existing cable-moored platform "Kulluk." A scale of 1:45 can be used to the relate the test platform to "Kulluk." Table 1 lists the principal dimension of both "Kulluk" and the test platform. A detailed drawing of the test platform is given in figure 5.

As discussed by Matsuishi and Ettema (1985a) a floating cable-moored platform can be considered to be affected by three linear restoring forces or moments.

(a) A horizontal mooring force arising from the spring stiffness of the model. Three values of spring stiffness were used in these tests; $K_s = \infty$, 1.7kN/m, 0.5kN/m. The latter two stiffnesses were obtained by means of leaf springs in the mooring harness.

(b) A vertical foundation reaction force, opposing heave motion, due to buoyancy; K_n = 17.3kN/m.

(c) A foundation reaction moment, opposing pitch motion, again due to buoyancy; k_p = 35.1kNm/degree.

3. Instrumentation.

The platform was instrumented in two different ways: (a) for K_s being non-infinite (i.e., the platform was "moored"); and (b) for K_s infinite (the platform was "fixed").

When "moored", the platform was connected to an instrument beam by way of a linear mooring harness and a load cell (see figure 5). The mooring harness comprised a pair of elastic leaf springs (to provide K_s), a spline bearing, stroke bearings and universal bearings, as shown in figure 7. The harness simulated accurately the motion of a floating, moored platform. Horizontal mooring force was measured using a 490-Newton NISHO DENKI LMC-3502-50 load cell which connected the mooring harness to the instrument beam. Yawing and

swaying of the moored platform were restricted by two vertical rods located at the fore and aft of the platform (see figure 8). The 10mm diameter rods were constrained to slide in 10.5mm wide slots (see figure 9). Thus the moored platform had three degrees of freedom for motion: heave, pitch and surge.

Heave and pitch motions were measured by means of two linear voltage displacement transducers (LVDT's), which sensed the vertical motion of the platform at two positions, fore and aft. The LVDT's were excited using 12 volts with a full stroke range of 0.15m.

Vertical and horizontal accelerations of the moored platform were measured with three 2g($19.6ms^{-2}$) KYOWA ASQ-2BL accelerometers.

The "fixed" platform ($K_s = \infty$) was connected directly to a load cell which was, in turn, bolted to the instrument beam (see figure 10). The horizontal and vertical forces, and the pitching moment experiences by the fixed platform were measured using a 196-Newton and 98-Newton-meter NISHO DENKI LMC-4107-20 load cell.

The locations of the measuring sensors and the positive directions of recorded data are shown in figure 11. The output voltages from the measuring sensors were scanned with a digital voltmeter. The digitized data were serially transmitted to IIHR's HP-1000E computer system, and there stored on disc. The data acquisition band width was 120Hz, though each channel was sampled at a rate of either 7 or 10Hz.

4. Calibration of transducers.

For each of the data-logging transducers, the zero level and sensitivity were determined before each test.

Each of the load cells and accelerometers had their output voltage, v, measured for an amplifier-created calibration strain ε_c. The sensitivity, S, of each transducer was evaluated as

$$S = (v/\varepsilon_c)C \qquad (1)$$

where C is a predetermined ratio of strain to the force or acceleration experienced by the transducer.

Sensitivities of the LVDT's were evaluated by measuring the voltage change for a given displacement of the transducer rod.

The sensitivity of the carriage velocity measurement was determined by correlating the output voltage with the mean carriage velocity as measured with a length scale and stop watch. Calibration coefficients are listed in table 2.

B. Model Ice

Ice sheets were grown from a 0.7% by weight urea solution by the "wet seeding" procedure described in detail by Matsuishi and Ettema (1985a). Sheets were grown to three nominal thicknesses (20, 30 and 40mm). After seeding had occurred, the cold room was adjusted for maximum cooling rate until the ice sheet had grown to 85% of the desired thickness. At that time the room temperature was raised to allow the ice sheet to temper (i.e., to weaken).

The flexural strength, σ_f, and the flexural modulus of elasticity, E_f, were monitored during the warm-up period until σ_f attained a prescribed value (25kPa or 40kPa). The load F to fail a cantilever beam of length ℓ, width b, and thickness h, in downwards flexure was used to estimate σ_f:

$$\sigma_f = \frac{6F\ell}{bh^2} \tag{2}$$

Two to three cantilever beams were tested at several locations around the ice sheet in order to obtain a representative mean value of σ_f at intervals as the sheet weakened.

The flexural elastic modulus, E_f, was determined by measuring the increment δ of the vertical deflection of the ice sheete due to small increments of a point load ΔP, applied at the center-point of the ice sheet. Thus

$$E_f = \frac{0.188(1-\nu^2)}{\rho_w g h^2} \left(\frac{\Delta P}{\delta}\right)^2 \tag{3}$$

where ν = Poisson's ratio for ice (taken to be 0.3); ρ_w = density of urea solution (= 1000 kg/m^3); and g = gravitational acceleration (= 9.81ms^{-2}). The data associated with each ice sheet are given in table 3.

C. Preliminary Tests.

A number of tests were conducted to determine natural frequencies and the logarithmic decrement of the moored platform surge, heave and pitch oscillations both in open water and in ice conditions. The results are tabulated in table 4. Openwater tests had been conducted previously by Matsuishi and Ettema (1985a) who had concluded that additional hydrodynamic forces due to movement of the push blade used for driving ice sheets were negligibly small. The coefficient of friction between the platform and the ice was measured, using a range of normal pressures.

D. Test Procedures.

A total of 42 tests were conducted; 15 using the fixed platform, 7 using the moored platform with K_s = 1.7kN/m, and 20 using the moored platform with K_s = 0.5kN/m. For each test series, the ice sheet was pushed with a constant velocity against the platform by the carriage. The velocities used were 0.02, 0.04, 0.1 and 0.2m/s. The relationships between model and prototype values of ice sheet speeds are given in figure 12, while the relationships between forces and moments for model and prototype are shown in figure 13.

III. PRESENTATION OF RESULTS

A. Data

Individual time series from the tests are presented in a separate addendum to this report. (Examples of time series are shown in Appendix 1.) The data obtained from the digital voltmeter were converted from voltages into "engineering" values (N for force, ms^{-2} for acceleration, mm for heave, degrees for pitch) by means of a simple computer program. The time histories were also analyzed to give the temporal mean, the standard deviation about that mean, and the maximum and minimum values for each signal. Table 5 gives the results for the "fixed" platform tests, and table 6 for the "moored" platform tests.

B. "Fixed" Platform

Figures 14 through 17 show the effect on horizontal force of velocity. Note that, as in all graphs of results, the mean force and the mean plus two standard deviations are plotted (following the practice of Matsuishi and Ettema, 1985a). It can be seen that horizontal surge force increases with velocity. Similar trends are observed for vertical (heave) force (figures 18 through 21) and pitch moment (figures 22 through 25). Horizontal force, vertical force, and the magnitude of the pitching moment all increase with increasing ice thickness (see figures 26 through 28). The effect of ice strength is less clear, but would appear to indicate that both forces and the pitching moment increase with ice increasing strength.

C. "Moored" Platform

Figures 29 through 33 show the variation of horizontal (surge) force with velocity for the moored platform. The mean surge force appears to increase with velocity, though not always monotonically. There is a possibility of a minimum force at some intermediate velocity. This minimum is more evident if one considers the variation of the mean force plus two standard deviations with ice velocity. This is discussed further in Section IV below. Figures 34 through 36 show the effect of ice thickness on mooring force; mooring force clearly increases with increasing ice thickness. Note, however, that for the 40 mm ice thickness K_s = 1.7 kN/m, while for all other thicknesses K_s = 0.5 kN/m.

D. Qualitative Data

As well as collecting time series of loads, displacements and accelerations, visual data was also gathered. An underwater video, viewing the underside of the model platform, was taken for each test significant ice underride occurred in all cases, which is cause for concern since underriding ice may foul drill string or mooring lines. Above water videos were also taken of each test. After each test, any ice lodged under the platform was collected and photographed (see, as an example, figure 37).

IV. DISCUSSION

A. Observations

A number of qualitative observations can be made with regard to ice and platform behavior during the tests.

1. Modes of ice fracture

As expected, ice fractured circumferentially as it thrust against the platform (see figure 38). After downward flexure had produce a circumferential crack ice segments were further broken by radial cracks. The resulting ice pieces were then shored down the hull and clearing from beneath it occurred in one of three ways. They were either swept past the sides, or under the bottom of the platform, or it rotated back under the oncoming ice sheet. The last clearing mechanism leading to the formation of a ridge or collar of broken ice that ringed the platform and significantly affected the ice loads it experienced.

2. Platform motion

The platform, amidst a moving ice sheet, showed a fairly regular, though also stochastic, motion. The platform would pitch up at the point of impact and heave, while being shoved backwards. After a certain amount of motion it would lurch, or surge, forward rapidly, only to be shoved backwards again. Numerous smaller motions were superposed on this long term surge behavior. This behavior is discussed further in Section E, below.

3. Ice subduction

A major concern in any floating drilling structure is to avoid broken ice moving under the structure and fouling the drill string. In a cable moored system such as "Kulluk", a further concern is added; that of avoiding fouling of moored cables. Considerable ice under flow was observed in the tests conducted for this study, being most prevalent in thick ice conditions. Somewhat different behavior could be expected for the "Kulluk" platform, because of differences in a hull shape, particularly of the hull "skirt" (see figure 39). Thus while "Kulluk" would experience less ice underflow than the model

platform, it would experience higher forces, since ice could jam in the "skirt" angle and crushing may occur in that region.

B. Ice Thickness Effects

As noted in Chapter III above, for both the "moored" and the "fixed" platform all measured parameters (surge force, heave and pitch for the "moored" platform, surge force, heave force and pitch moment for the "fixed" platform) increased their mean and peak values monotonically with increasing ice thickness. This is as to be expected since for a given ice strength the load to break an ice sheet in downward bending increases. In fact, if one treats an ice sheet as approximately a simple beam one has

$$\frac{\sigma}{y} = \frac{M}{I} \tag{4}$$

where σ = the strength of the ice; y = half the thickness of the ice sheet; I = the second moment of inertia; and, M is the breaking moment. If we allow $I = bt^3/12$ (where b = breadth and t = thickness of the simple beam), then we have:

$$M = \frac{\sigma_y \cdot bt^2}{b} \tag{5}$$

since $y = t/2$. The moment required to break the beam is given by

$$M = F\ell \tag{6}$$

where F is the resultant force due to the platform acting on the ice, and ℓ is the appropriate moment arm (see figure 40). It is reasonable to assume that ℓ will be related to the characteristic length, ℓ_c, which is generally taken (e.g., IAHR 1980) as proportional to $t^{3/4}$. Thus, we might expect that

$$F \propto t^{1.25} \tag{7}$$

However, two factors should be considered. First, no account has been taken of dynamic effects, nor has the effect of the skirt on the platform been considered. Second, the above analysis is simple and only a two-dimensional

approximation. Ralston (1980) provides a three dimensional plasticity solution expressing the horizontal and vertical forces as second-order polynomial functions of ice thickness, while Enkvist (1983) suggests that the resistance of the ice is directly proportional to the ice thickness. Given the complexity of the platform geometry, no simple relationship between forces and thickness should be expected, but the upward curvature apparent in almost all of figures 26 through 28 and 34 through 36 suggest a relationship of the form:

$$F_x,\ F_y,\ M_z \ \alpha\ (t)^n \qquad (8)$$

where $n \tilde{>} 1$.

C. Ice Velocity Effects

For the fixed platform, a general trend appears to be that both mean and peak values of heave force, surge force and pitch moment increase monotonically with increasing ice velocity. In some cases, however, it appears that a minimum in these parameters may occur at $V \simeq 0.05$ m/s; as for ice thickness = 30 mm and strength = 25 kPa for the fixed platform (figures 15, 19, 23). This may be related to resonance and dynamic effects, or could simply be the result of scatter. One would expect the forces to increase with ice velocity if, as was the case here, the mode of ice failure remained the same (viz., downward fracture) through the range of velocities investigated because forces associated with flexural breaking and submergence of ice increase (see for example, Schulson 1987).

For the moored platform, the situation is more complex as would be expected, given the more dynamic nature of the experiments. Thus, although for three cases (t = 40 mm, S = 25 kPa; t = 20 mm, S = 40 kPa; t = 30mm, S = 40 kPa) the heave appears to increase monotonically with velocity, this is not the case in the other two cases (t = 30 mm, S = 25 kPa; t = 20mm, S = 25 kPa). Similar inconsistencies are apparent for the surge force and pitch angle. It appears that the stochastic nature of the ice fracture process overrides any deterministic trends which might be occurring.

D. Mooring Stiffness Effects

Including the work of Matsuishi and Ettema (1985a), three tests have now been performed for three mooring system stiffnesses ($K_s = \alpha$, 1.7 kN/m, 0.5 kN/m). As figure 41 shows there appears to be a minimum of surge force as a function of inverse mooring stiffness ($1/k_s$). This is a very important result, particularly for the design engineer, as it suggests that there may be an optimum mooring stiffness which provides minimum loads and accelerations on the platform. This result requires further investigation. In particular, it is not clear precisely what factors contribute to this minimum. Future experiments are planned to elucidate this matter.

E. Dynamic Response

In order to determine the dominant frequencies of mooring loads, platform motions, and the controlling failure modes of the ice as it moved against the platform, spectral analysis of time-histories was performed using a fast fourier transform computer program. The frequency spectrum for each test was then compared with the calculated breaking frequency f_b. f_b is calculated by dividing the ice impact velocity, V, by the average length of broken pieces l_b, thus:

$$f_b = \frac{V}{\ell_b} \tag{9}$$

In order to highlight certain trends the following discussion will concentrate on cross-cuts through the tests. Four moored platform tests (all with ice thickness = 30 mm and ice strength = 25 kPa) are considered with impact velocities ranging from 0.02 to 0.20 ms^{-1}. Similarly, four fixed-platform tests are considered (see Table 7).

1. Moored platform dynamic response

Figures 42 through 45 show the frequency power spectra for mooring force (or surge displacement), F_x, and pitch angle, θ, for tests P301 through P304. Relevant data are listed in table 7. Figure 41 shows that for test P301 both F_x and θ exhibit a dominant peak at $2\pi f = 0.7$ which is approximately $f_b/2$. Mooring force also shows a peak at $f = f_b$. For P302, F_x shows a double peak

at $2\pi f \simeq 1.0 - 1.2$, while θ shows a peak at $2\pi f \simeq 2.0$ which is associated with f_b. The double peak in the mooring force spectrum appears to be associated with the natural surge frequency of the platform, f_n; $2\pi f_n$ is approximately 1.4. The mooring force peak is rather broad banded, a trend which persists for all data and is a result of the markedly stochastic nature of the ice fracture process around the platform. In test P303, there is a secondary peak on the mooring force spectrum at $2\pi f \simeq 4.2$ which corresponds to f_b but again, the primary peak is associated with the natural frequency. In the pitch spectrum, the primary peak is at $2\pi f_b$. P304 continues this trend. Again, surge is dominated by the platform's resonant frequency. In the pitch spectrum, three peaks are evident, which correspond to $f_b/3$, $f_b/4$ and $f_b/5$. To express this physically they represent vibrations associated with every third, fourth and fifth fracture process.

The trend for the moored platform would thus appear to be as follows. When breaking frequency, f_b, is less than the platform's natural frequency of surge oscillation amidst ice, f_s, the dominant frequency of mooring-force oscillation coincides with an integer fraction of f_b; usually $f_b/2$. Physically, this means that the platform is shoved back by the ice, which all the white fails flexurally until mooring forces exceed imposed ice forces and the platform surges forward, to be shoved back once again.

When f_b equalled or exceeded f_s, the dominant frequency of mooring force, and platform surge, was f_s. Physically, the moored platform acted as if it were a plucked violin string. When released from a position of maximum surge displacement, mooring forces caused the platform to spring forward, impacting the onward thrusting ice sheet in a brief series of and breaking, heavily damped vibrations. Pitch oscillations of the platform occurred primarily at the breaking frequency (or some fraction thereof). It should perhaps be noted that there are a number of inaccuracies inherent in the frequency analysis. Data was gathered at 7 or 10 Hz, thus higher frequencies than this are not analyzed. Similarly, test length was at most 400 seconds, so very low frequency effects will not be captured. Nonetheless, it does seem clear that the two major loading modes on the platform are the long term surge and the breaking of the ice.

2. Fixed platform dynamic response

Figures 46 through 49 show the frequency power spectra for surge restraining force (F_x) for tests P301F through P304F, with associated data in table 7. The spectra are more broad banded than for the moored platform, which is a result of the lack of degrees of freedom for the fixed platform. In a sense, the fixed platform was unable to tune its responses to either the forcing frequency, or to a natural frequency of motion. P301F shows a secondary peak at f_b with the primary peak at $f_b/2$. In P302F there is a very broad peak, with the upper frequency corresponding to f_b. A similar situation is evident for P303F. The smaller, higher frequency peak corresponds to f_b, and the trailing peak may be associated with the clearing of rubble from around the platform. P304F show another double peak, centered on $f_b/2$. In contrast to the moored platform there is no long period surge peak. This is to be expected since the platform is fixed. Again the breaking of the ice appears to be an important feature in the ice fracture process.

V. CONCLUSIONS

The following conclusions were drawn from the study:

1. When impacting the platform, ice sheets fractured circumferentially. Significant amounts of broken ice passed under the platform, especially for the thicker ice sheets.

2. For both "moored" and "fixed" platform tests, surge force, heave force and pitch moment (or heave displacement and pitch angle for the "moored" platform) increased monotonically with increasing ice thickness. The exact relationship between force and thickness is unclear, because of complexities in the interaction geometry, but is of the form

$$F \alpha t^n$$

where $n \tilde{>} 1$.

3. The general trend for the "fixed" platform was for surge force, heave force and pitch moment to increase monotonically with ice velocity. The

few exceptions to this are probably due to scatter, though resonance effects cannot be dismissed.

4. In contrast, for the "moored" platform the effect of ice velocity on surge force, heave displacement and pitch angle is clearly compllicated by resonance effects.

5. The surge force experienced by the platform exhibits a minimum as stiffness decreases from infinity. The minimum occurs at $K_s \approx 1$KN/m.

6. Fourier analysis of the time series show that for the "fixed" platform the dominant frequency is the breaking frequency of the ice, f_b, or some whole number fraction thereof.

7. The "moored" platform also showed the breaking frequency, or a fraction thereof, to be dominant for both heave and pitch. However, the surge force power spectrum was dominated by the natural surge frequency of the platform.

REFERENCES

Enkvist, E. (1983), "Level Ice Resistance," VIIth Graduate School on Ships and Structures in Ice, Helsinki, Chapter XV.

Frederking, R. and Schwarz, J. (1982), "Model Test of Ice Forces on Fixed and Oscillating Cones," Cold Regions Science and Technology, Vol. 6, pp. 61-72.

Frederking, R. (1984), "Exploration and Production Concepts and Projects for Arctic Offshore," Proc. IAHR Symposium on Ice, Hamburg, V. 4, pp. 387-411.

Hnatiuk, J. and Wright, B.D. (1984), "Ice Management to Support the Kulluk Drilling Vessel," Proc. 35th Annual Technical Meeting of Petroleum Society of CIM, Calgary, Paper No. 84-94, pp. 333-365.

Loh, J.K.S. and Stamberg, J.C. (1984), "New Generation Arctic Drilling System: Overview of First Year's Performance," Proc. 16th Offshore Technology Conference, Houston, Paper No. 4797.

Matsuishi, M. and Ettema, R. (1985a), "The Dynamic Behavior of a Floating Cable-Moored Platform Continuously Impacted by Ice Flows," Iowa Institute of Hydraulic Research, IIHR Report No. 294.

Matsuishi, M. and Ettema, R. (1985b), "Ice Loads and Motions Experienced by a Floating Moored Platform in Mushy Ice Rubble," Iowa Institute of Hydraulic Research, IIHR Report No. 295.

Ralston, T. (1980), "Plastic Limit Analysis of Sheet Ice Loads on Conical Structures," Physics and Mechanics of Ice, ed. p. Tryde, IVTAM Symposium, Copenhagen, pp. 289-308.

Working Group of the IAHR Section on Ice Problems (1980), "Standardisation of Testing Methods for Ice Properties," J. Hydraulic Research, Vol. 18, 153-165.

Table 1

Principal Dimensions of the Test Platform and "Kulluk"

		Test Platform "Kulluk" (1/45 scale)	
Diameter at deck level	(m)	1.8	81.0
Diameter at load waterline	(m)	1.5	67.5
Diameter at base line	(m)	1.334	60.0
Depth	(m)	0.334	15.5
Draft	(m)	0.187	8.4
Displacement	(m^3)	0.271	24700
Cone Angle	(degree)	31.4	31.4

Table 2

Calibration Coefficients for Test Transducer

Transducer	Coefficient	
Load Cell	17.62 N/volt	
Moored Platform	LVDT #1	12.7 mm/volt
LVDT #2	12.7 mm/volt	
Surge Force	7.85 N/volt	
Fixed Platform	Heave Force	7.85 N/volt
Pitch Moment	7.85 N/volt	

Table 3

Ice Sheet Data

Sheet No. (mm)	Thickness (kPa)	Strength, σ_Y	E/σ_Y
P201	21	24	921
P202	21	25	1064
P203	20	27	881
P204	21	27	940
P301	28	26	435
P302	27	24	400
P303	28	26	220
P304A	28	25	150
P305	28	40	1453
P401	39	24	549
P301F	32	27	1443
P201F	21	24	4458
P302F	30	20	2100
P202F	20	25	4976
P203F	20	25	1569
P303F	30	20	1522
P304F	30	24	1171
P305F	30	39	780
P306F	30	40	1518
P307F	30	40	705
P308F	30	38	1418
P309F	30	41	1861
P401F	40	24	2131
P402F	39	24	1471
P403F	39	25	2207

Table 4

Natural Periods and Logarithmic Decrements
of Moored Platform

	Surge Displacement (k_s = 1.7 kN/m)	Surge Displacement (k_s = 0.5 kN/m)	Heave Displacement	Pitch Rotation
Natural Period, T (seconds)	3.00	4.50	1.41	1.17
Logarithmic Decrement, δ	0.29	0.25	--	0.55

Table 5

Test No.	Thickness (mm)	Velocity (m/s)	Strength kPa	$\overline{F}_H$	2σ	$\overline{F}_v$	2σ	$\overline{M}_p$	2σ
P301F	29	0.02	25	47.4	39.0	56.9	39.4	-29.9	40.8
P302F	30	0.04	21	41.3	23.0	45.7	32.6	-31.8	32.8
P303F	30	0.1	24	48.5	27.4	33.5	52.6	-26.4	39.6
P304F	30	0.2	24	51.9	43.2	40.4	105.0	-34.2	70.2
P305F	30	0.02	39	47.2	46.2	57.4	33.8	-33.1	35.0
P306F	30	0.04	38	49.4	33.0	68.1	34.2	-45.5	32.8
P307F	30	0.1	39	51.3	32.8	53.2	64.8	-39.8	48.5
P308F	30	0.2	38	77.8	69.4	29.1	88.4	-41.8	48.0
P309F	30	0.2	41	80.7	75.4	85.1	171.4	-65.0	114.8
P401F	40	0.02	24	78.3	92.0	75.3	59.0	-39.1	62.0
P402F	39	0.1	24	87.0	71.4	67.2	95.8	-49.4	77.2
P403F	39	0.2	25	102.2	116.4	73.1	173.0	-49.1	124.8
P201F	21	0.02	24	18.6	10.7	24.2	18.1	-16.0	13.8
P202F	20	0.1	24	24.5	15.4	28.8	27.4	-21.8	18.0
P203F	21	0.2	25	39.0	31.8	37.9	78.4	-32.8	48.8

Table 6

Moored Tests

Test No.	Thickness (mm)	Velocity (m/s)	Strength (kPa)	$\overline{F}$	2σ	$\overline{P}$	2σ	$\overline{H}$	2σ
P201	21	0.02	24	13.1	3.4	-	-	-	-
P202	21	0.04	25	21.1	12.8	-0.201	0.230	-1.446	0.876
P203	20	0.10	27	22.8	4.2	-0.223	0.176	-1.269	0.718
P204	21	0.20	27	28.6	1.6	-0.162	0.132	-0.811	1.202
P301	28	0.02	26	26.6	20.0	-0.285	0.22	-2.001	0.9
P302	27	0.04	24	23.2	8.2	-0.238	0.23	-1.399	0.92
P303	28	0.10	26	28.5	4.0	-0.219	0.52	-1.405	1.34
P304A	28	0.20	25	29.3	4.4	-0.252	0.12	-1.277	1.16
P305	28	0.02	40	27.0	20.4	-0.207	0.26	-1.56	1.12
P205	19	0.02	40	27.5	23.4	-.211	0.188	-1.514	.799
P206	19	0.04	18	21.6	9.76	-0.201	0.162	-1.413	.576
P207	19	0.04	39	18.1	18.9	-0.248	0.236	-1.664	.716
P208	20.5	0.10	41	37.2	4.94	-0.339	0.262	-2.265	1.166
P209	19	0.20	39	37.5	4.72	-0.360	0.148	-2.25	0.96
P306	30	0.04	40	71.0	45.6	-	-	-	-
P3010	28	0.02	36	50.8	51.8	-0.226	0.334	-1.616	1.65
P309	28	0.20	36	77.8	9.6	-0.455	0.412	-4.54	3.03
P308	28	0.10	36	72.7	13.4	-0.423	0.834	-3.87	4.38
P307	28	0.04	36	64.1	32.2	-0.250	0.524	-2.412	1.72
P371	37	0.02	28	172.8	95.0	-0.150	0.690	-1.92	1.65
P403	40	0.02	24	167.0	73.4	0.060	1.00	-2.42	3.68
P404	40	0.10	21	91.3	46.2	-0.286	1.26	-3.05	2.38
P405	40	0.20	21	124.3	55.4	-0.382	1.28	-3.97	4.80
P406	40	0.02	22	57.4	62.8	-0.364	0.40	-2.72	1.86
P407	40	0.02	20	47.8	33.4	-0.395	0.36	-2.31	1.26
P408	40	0.10	20	87.0	53.4	-0.374	1.26	-2.91	2.90

Thickness

20 mm - 4 at 25kPa, 4 at 40kPa, 1 at 18kPa
30 mm - 4 at 25kPa, 1 at 21kPa, 6 at 40kPa
40 mm - 7 at 25kPa

Table 7
Platform Dynamic Response

A: Moored Platform; f = 30mm, s = 25kPa

Test #	Velocity(m/s)	breaking length(mm)	f_g	$2\pi f_b$	surge $2\pi f_{dom}$	pitch $2\pi f_{dom}$
P301	0.02	110	0.18	1.13	0.7	0.7
P302	0.04	95	0.44	2.76	1.0-1.4	2.0
P303	0.10	120	0.83	5.22	0.8-1.4	4.5
P304	0.20	75	2.7	17.0	1.4	5.2,3.8,3.2

B: Fixed Platform; f = 30mm, s = 25kPa

	Velocity(m/s)	breaking length(mm)	f_b	$2\pi f_b$	$2\pi f_{dom}$
P301F	0.02	155	0.13	0.82	0.55
P302F	0.04	120	0.33	2.07	2.1
P303F	0.10	115	0.87	5.47	4.2
P304F	0.20	100	2.0	12.6	6.0

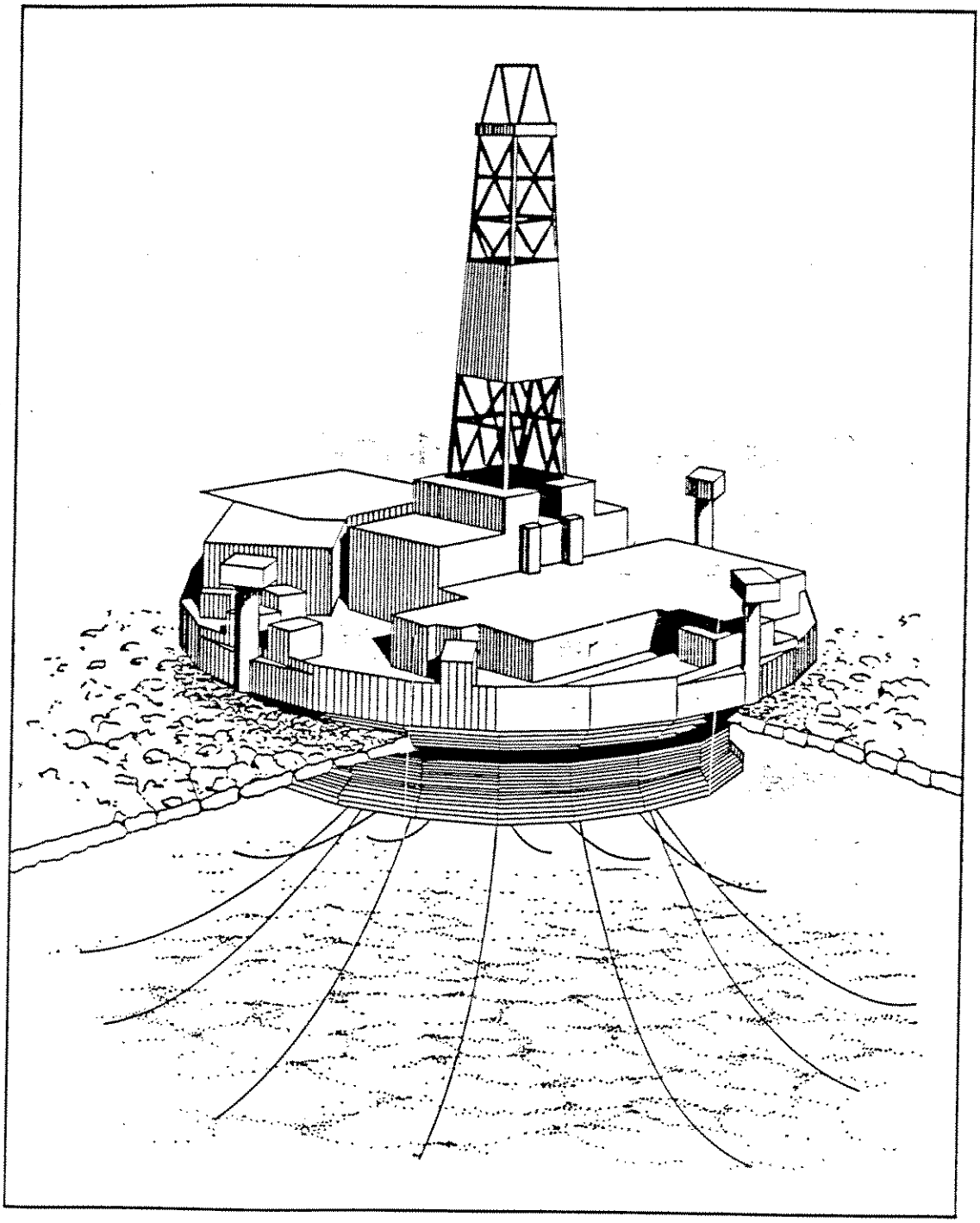

Figure 1. Conical Platform Similar to "Kulluk"

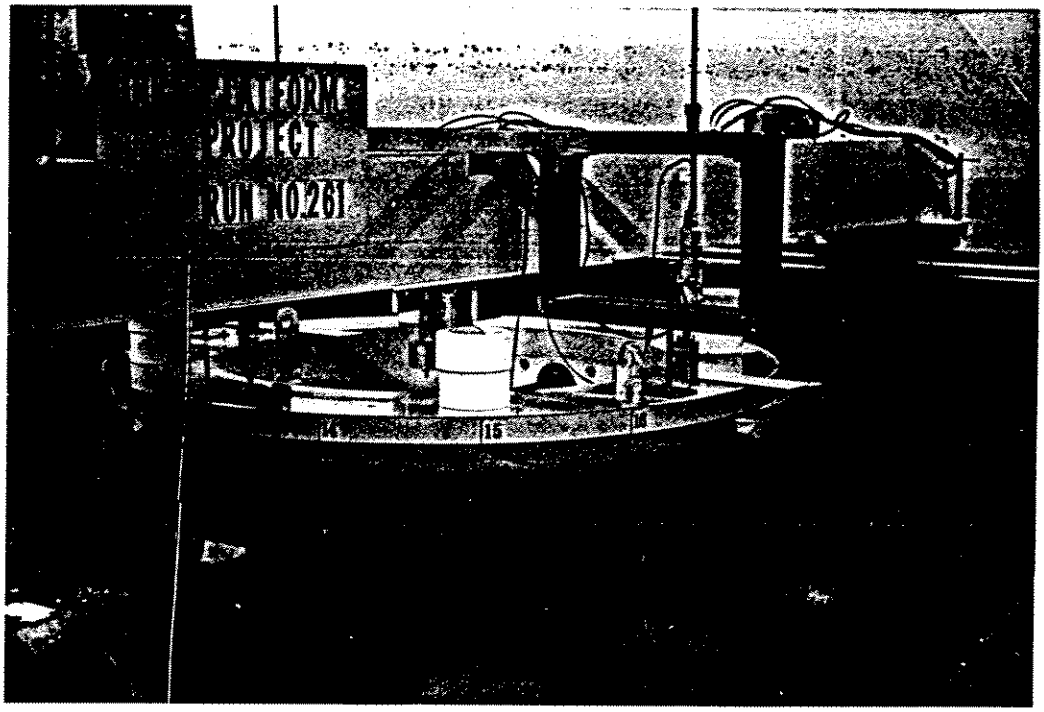

Figure 2. The Model Platform

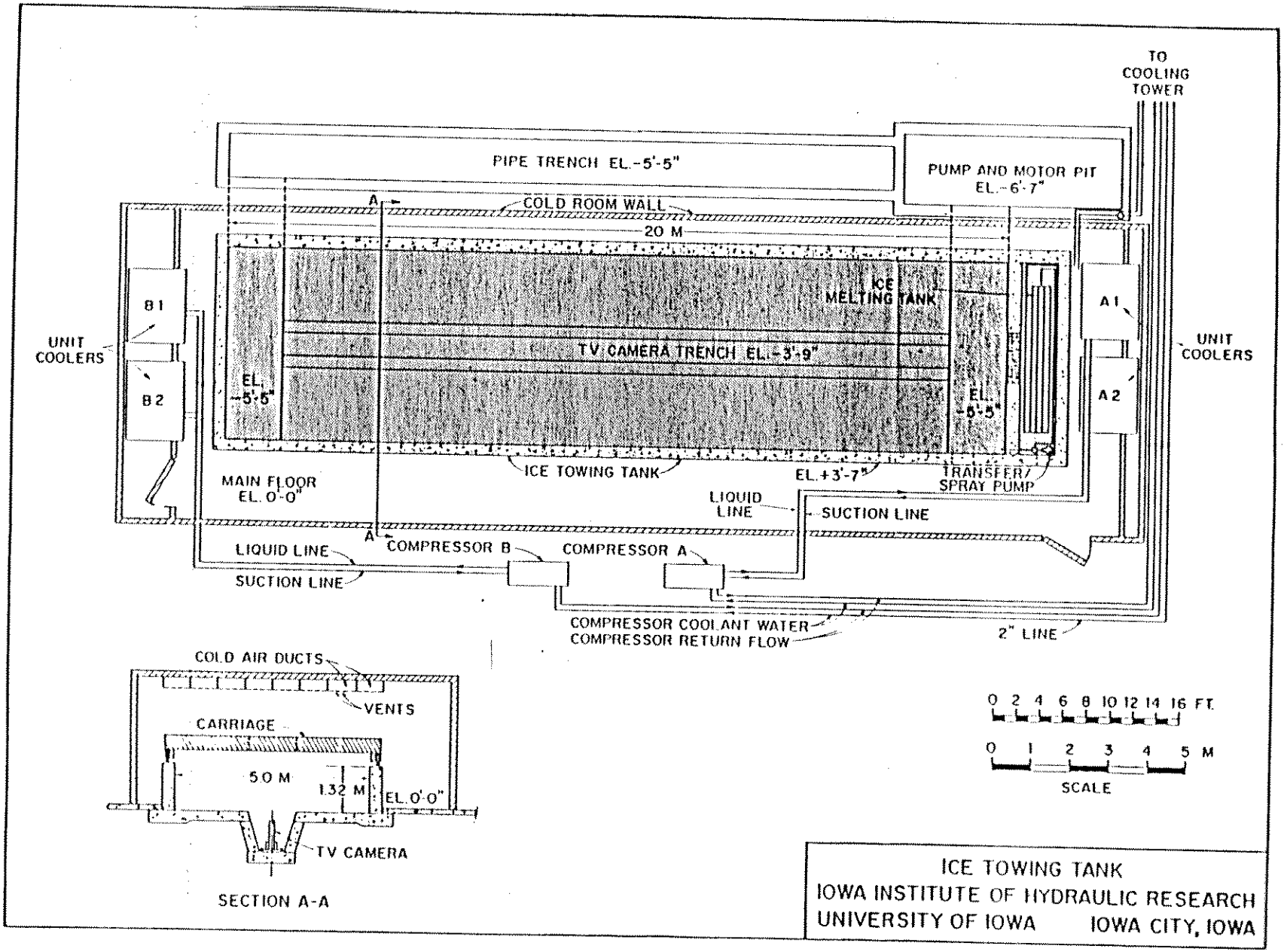

Figure 3. IIHR Ice Towing Tank Layout

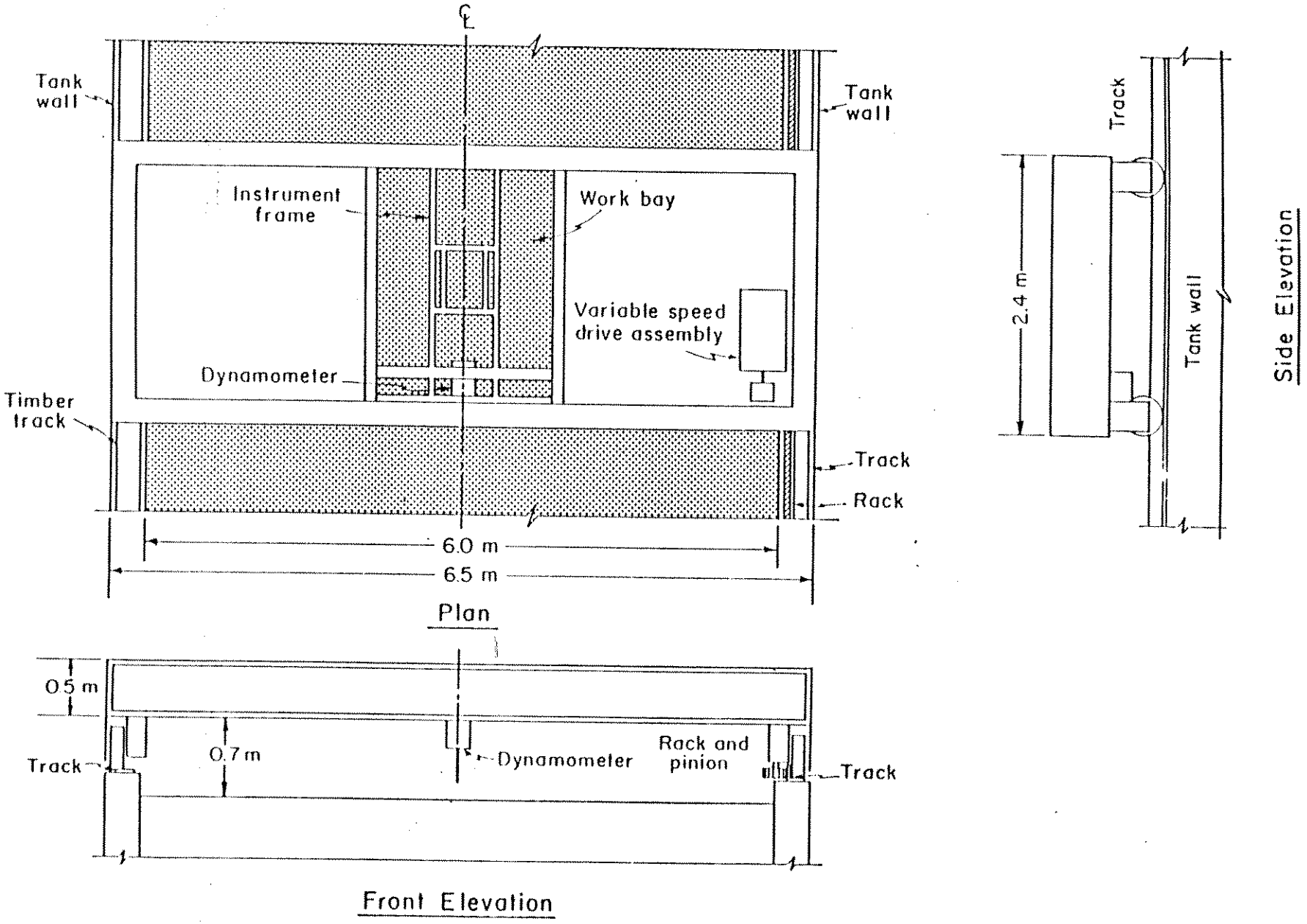

Figure 4. Towing Tank Carriage

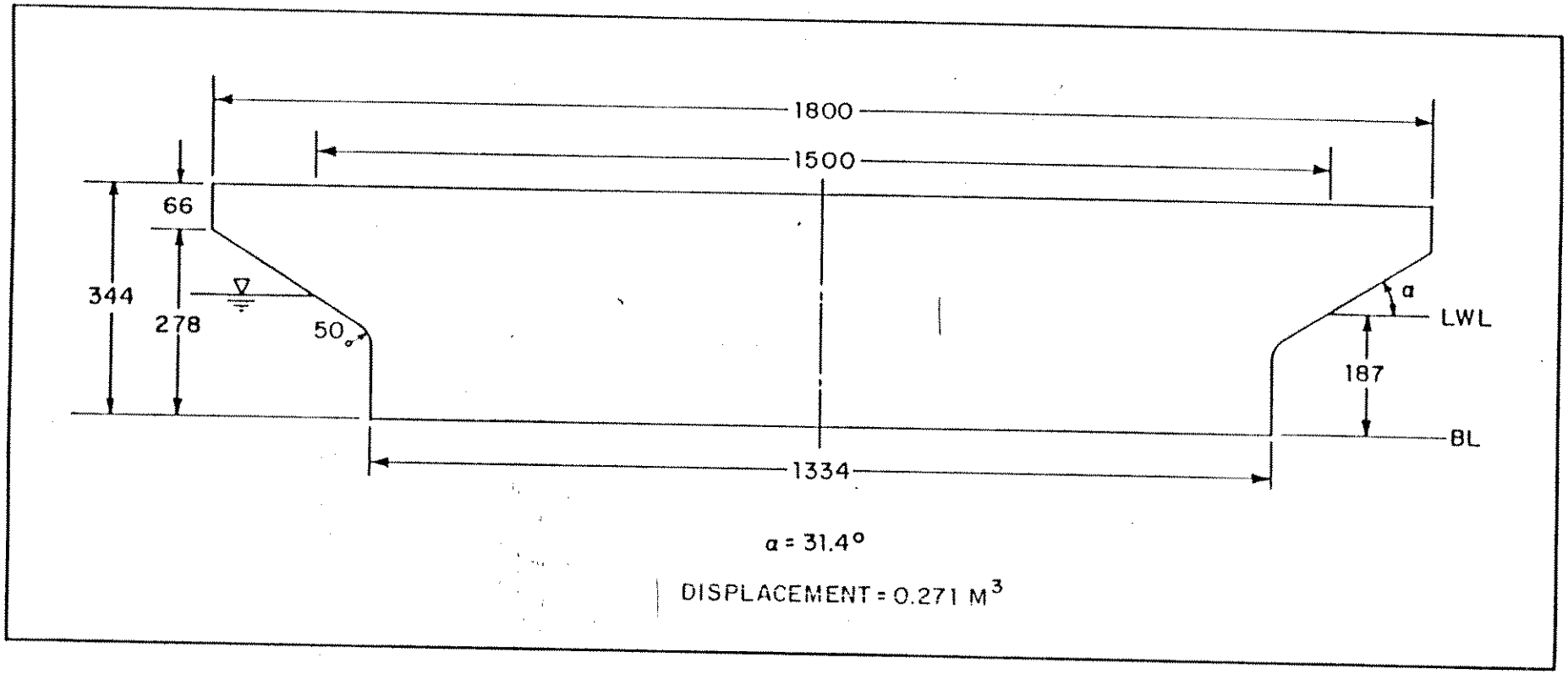

Figure 5. Detailed Drawing of Model Platform

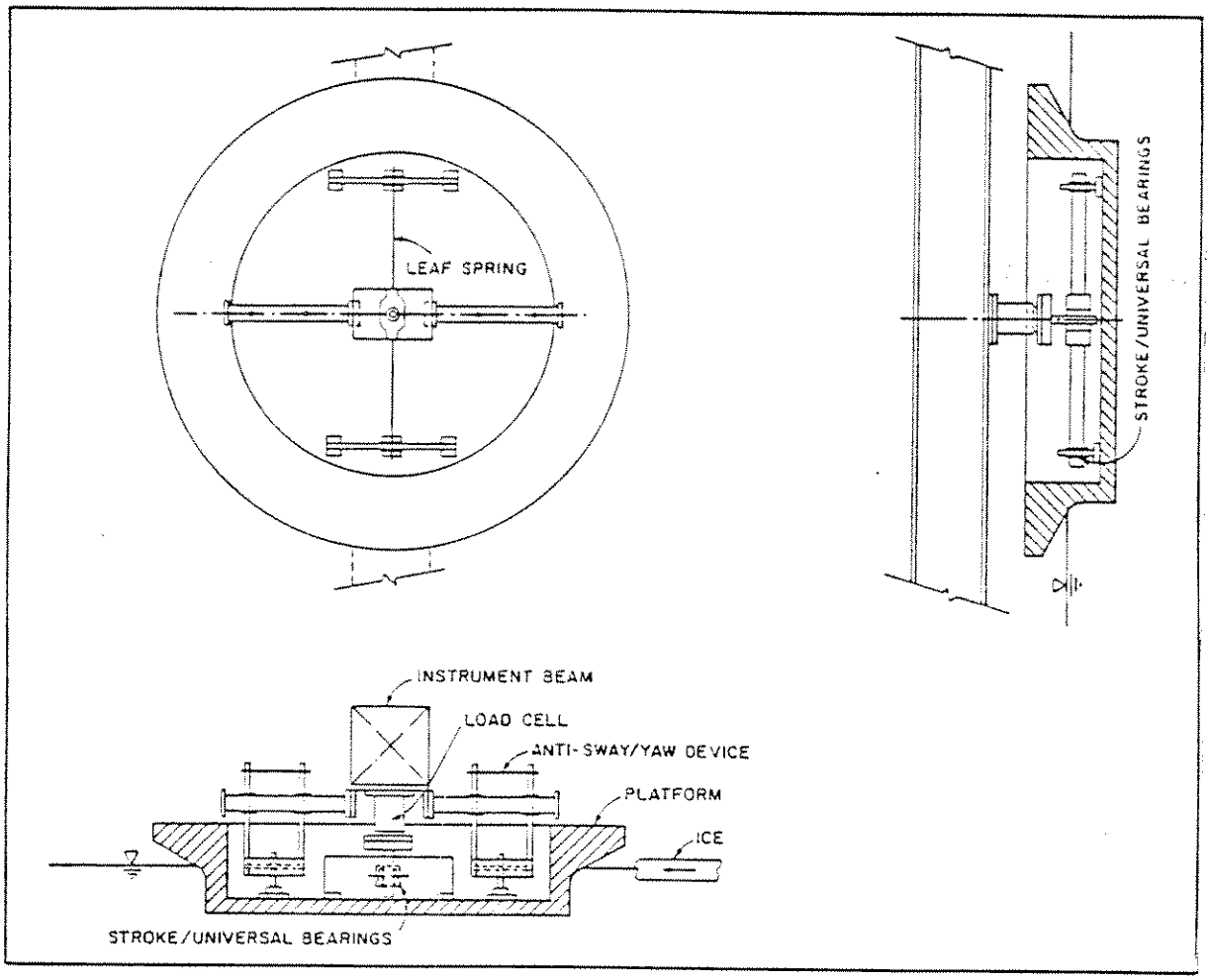

Figure 6. Instrumentation of Moored Platform

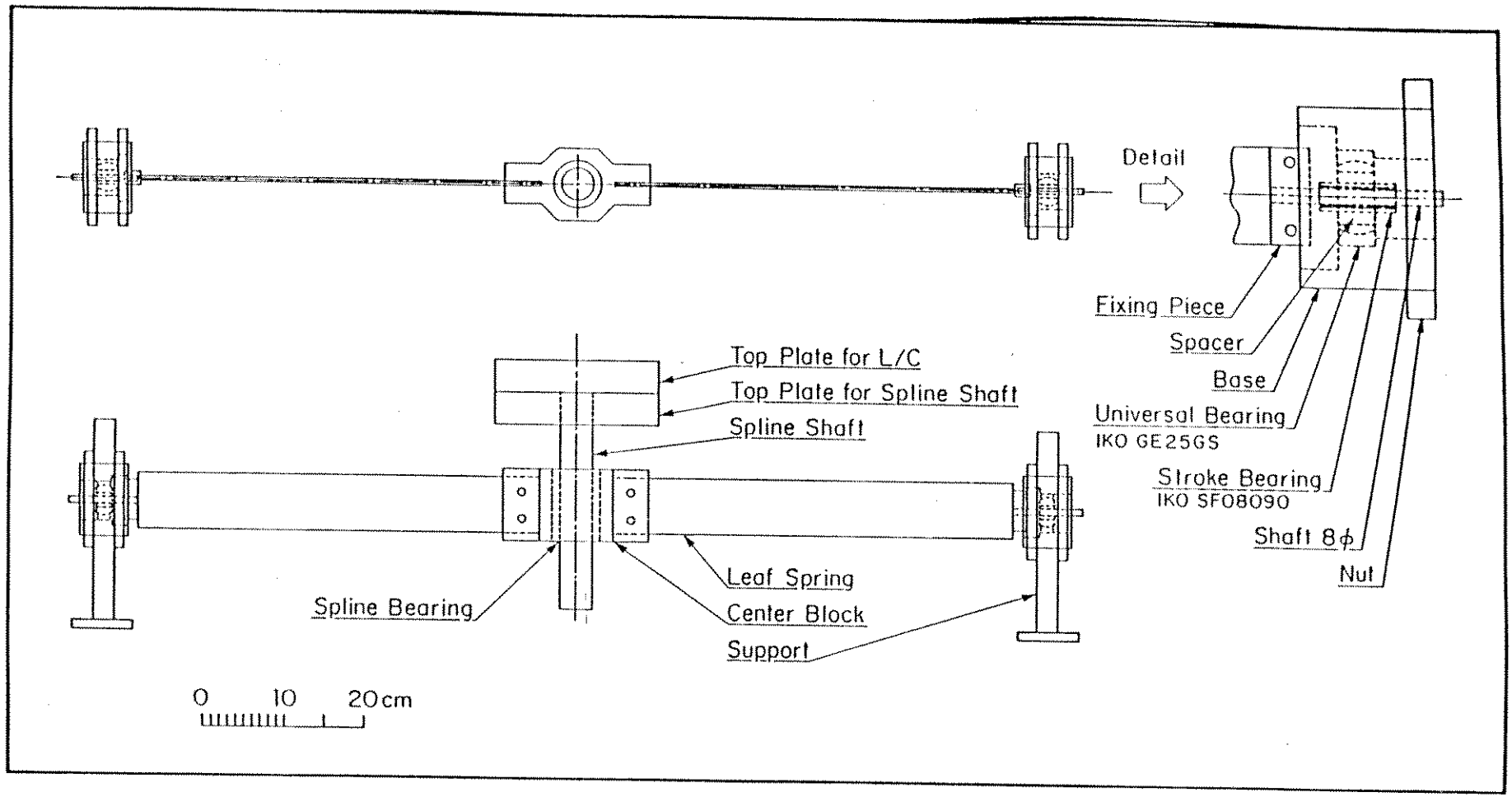

Figure 7. Details of Mooring Harness

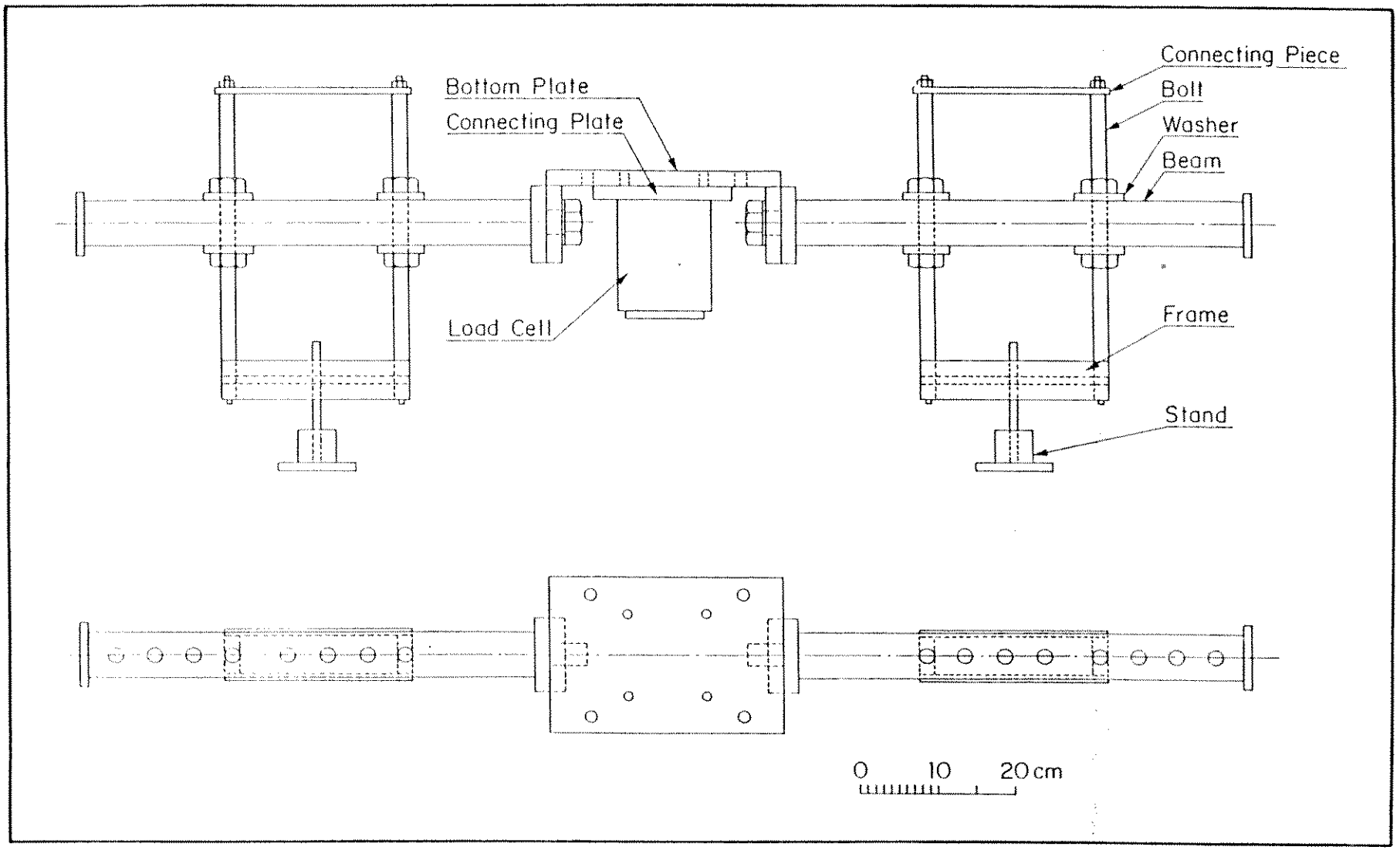

Figure 8. Details of the Sway and Yaw Restraining Device

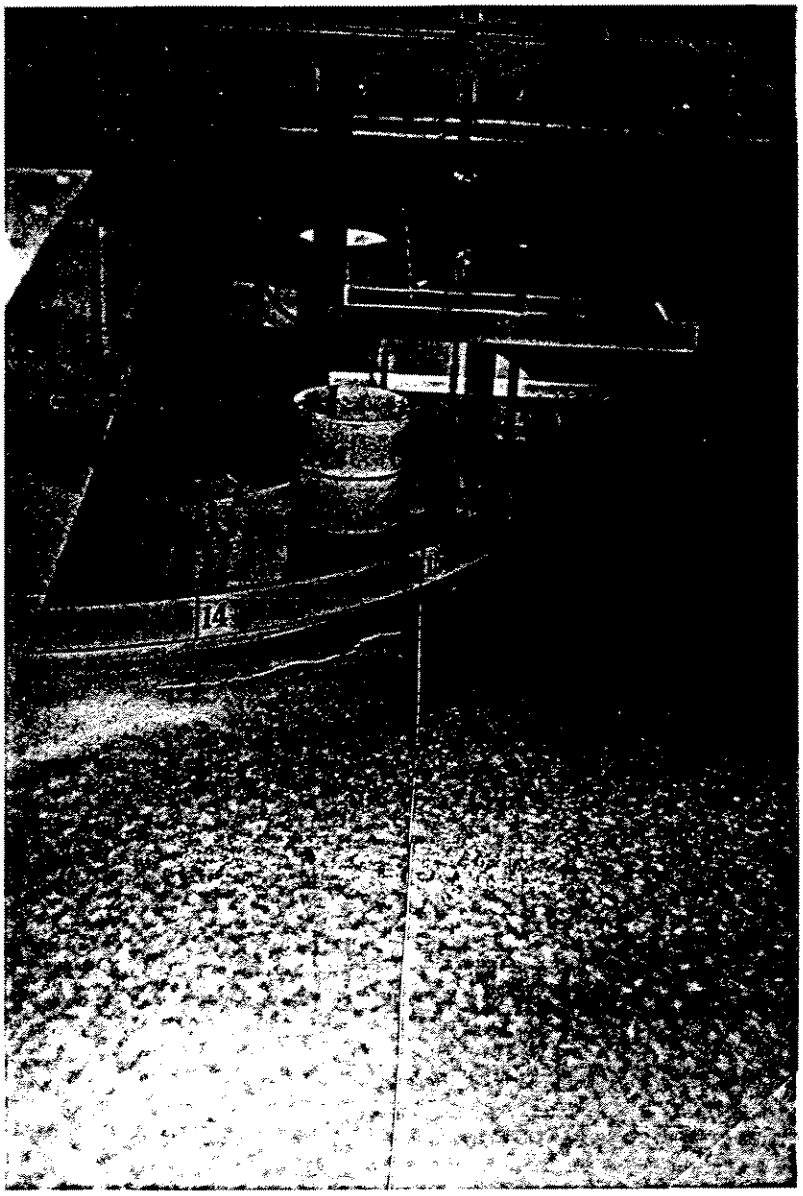

Figure 9. The Platform Showing Sway and Yaw Restraint

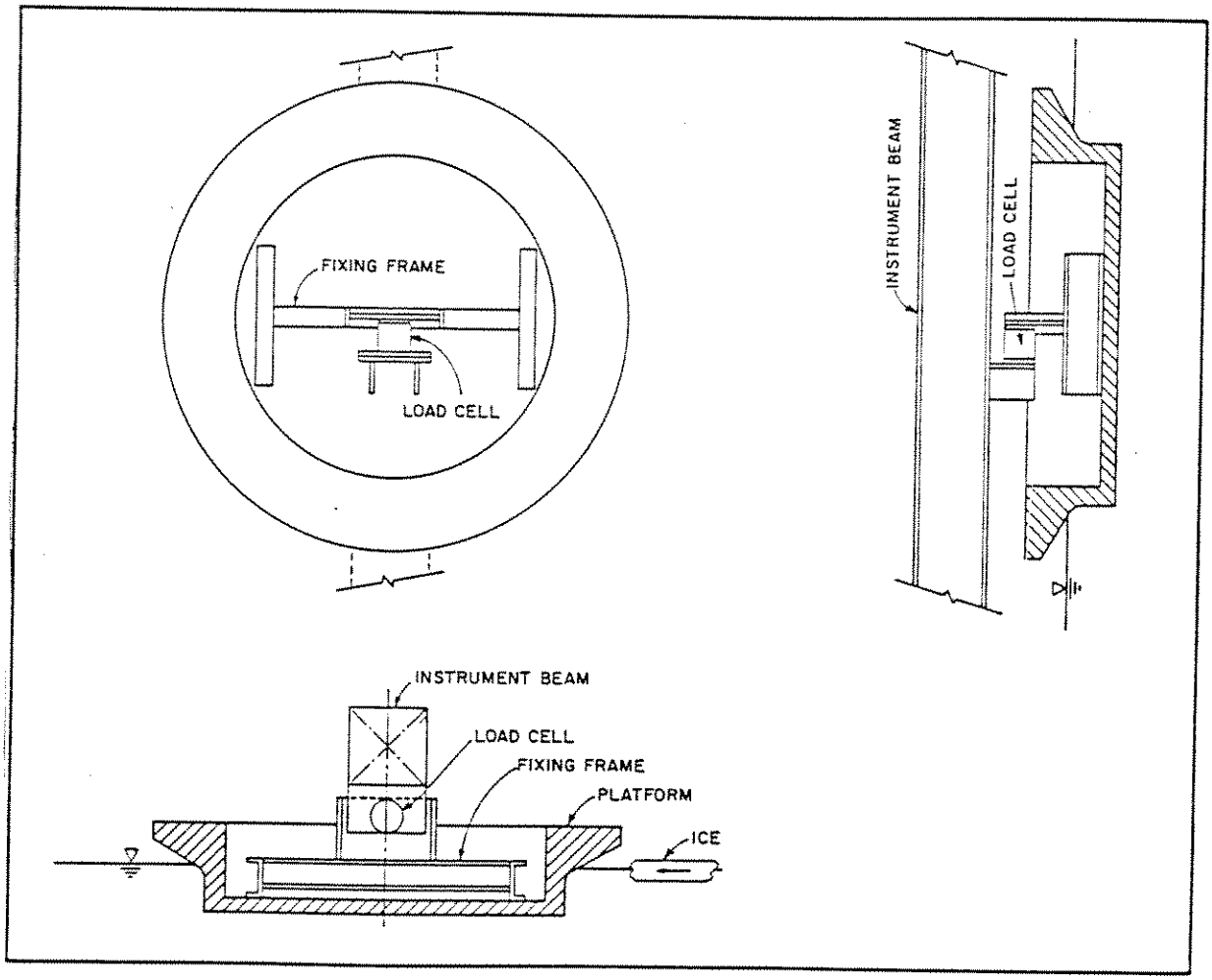

Figure 10. Instrumentation of Fixed Platform

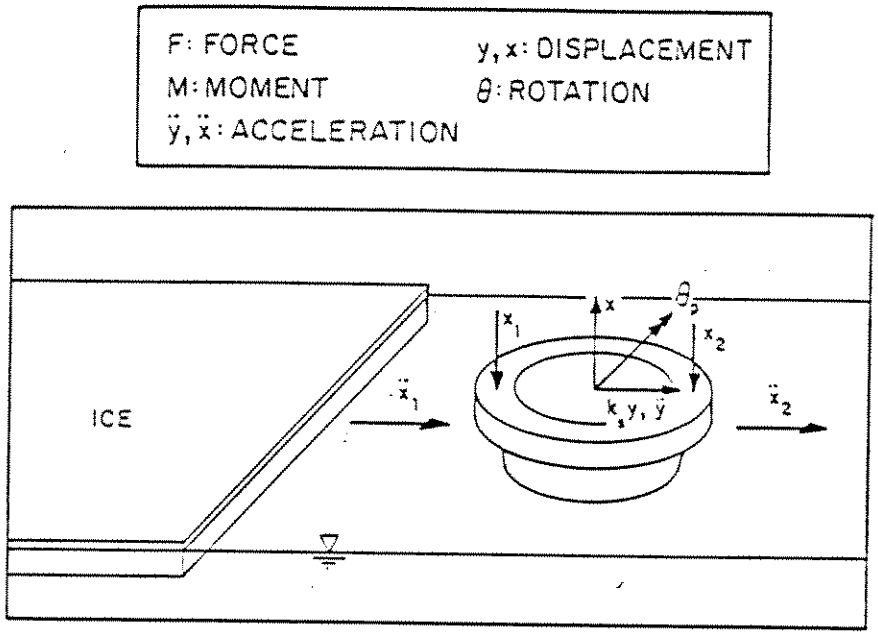

(a) MOORED PLATFORM

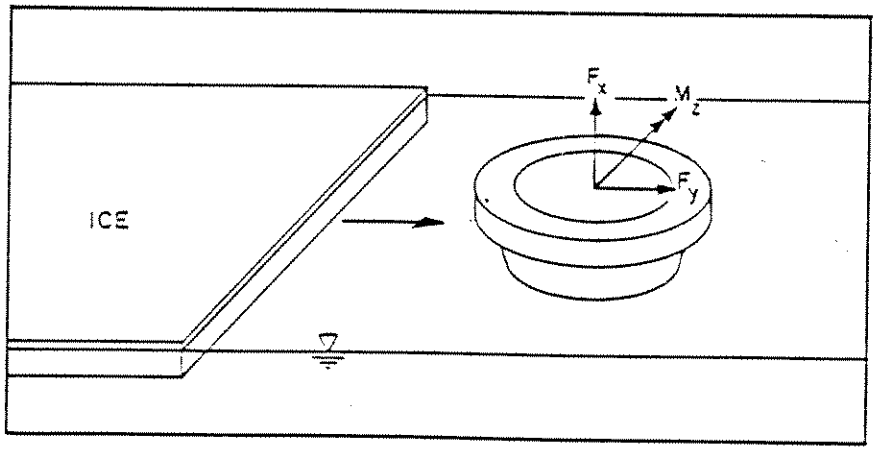

(b) FIXED PLATFORM

Figure 11. Locations of Measurements and Positive Directions

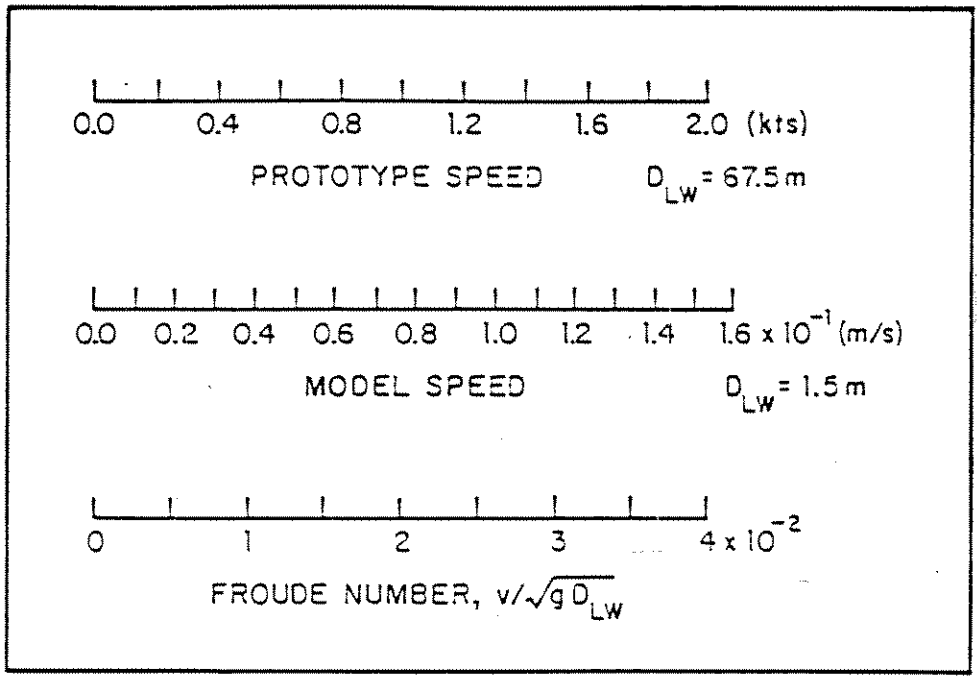

Figure 12. Relationships Between Model and Prototype Ice Impact Speed

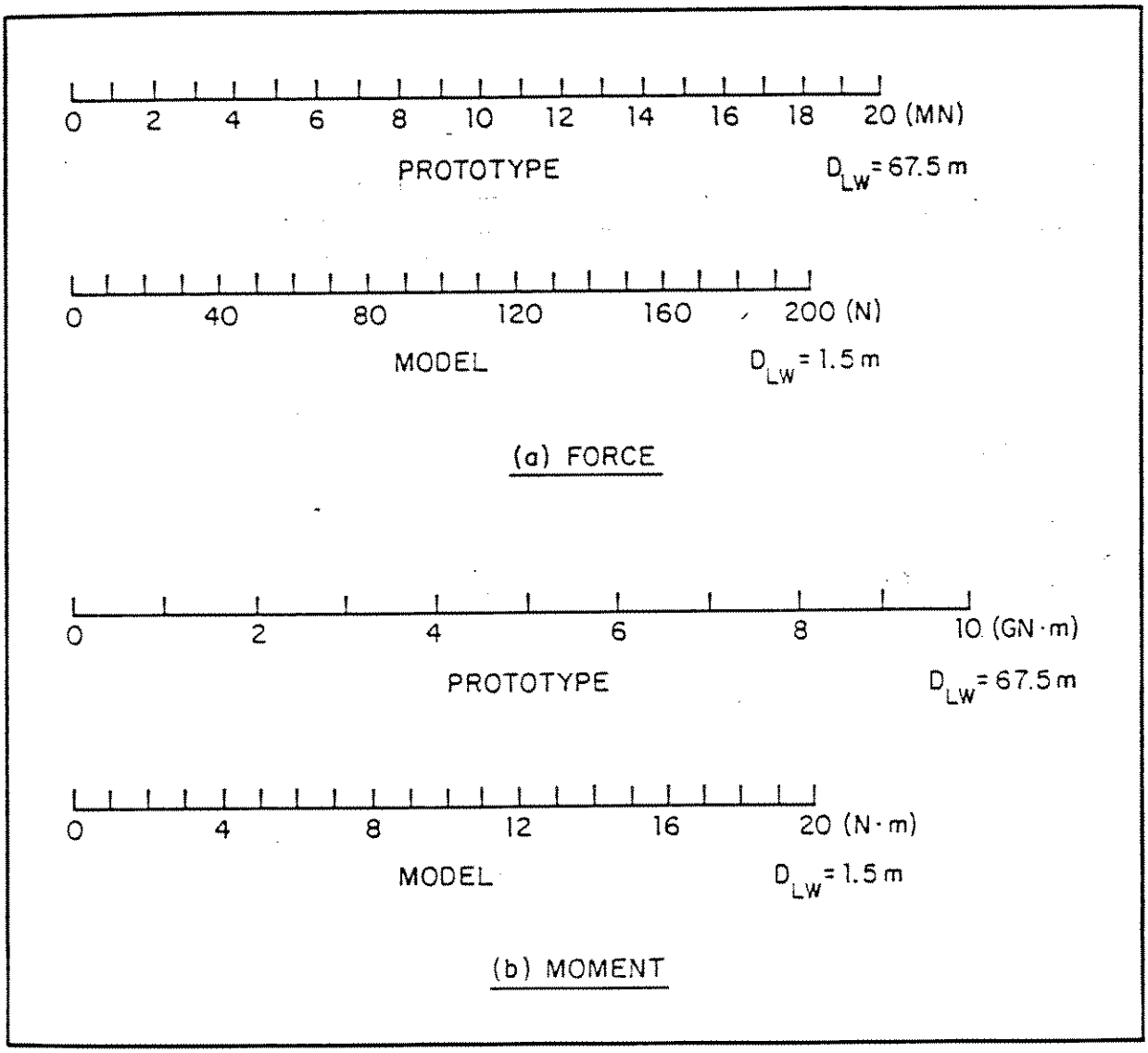

Figure 13. Relationships Between Model and Prototype Forces

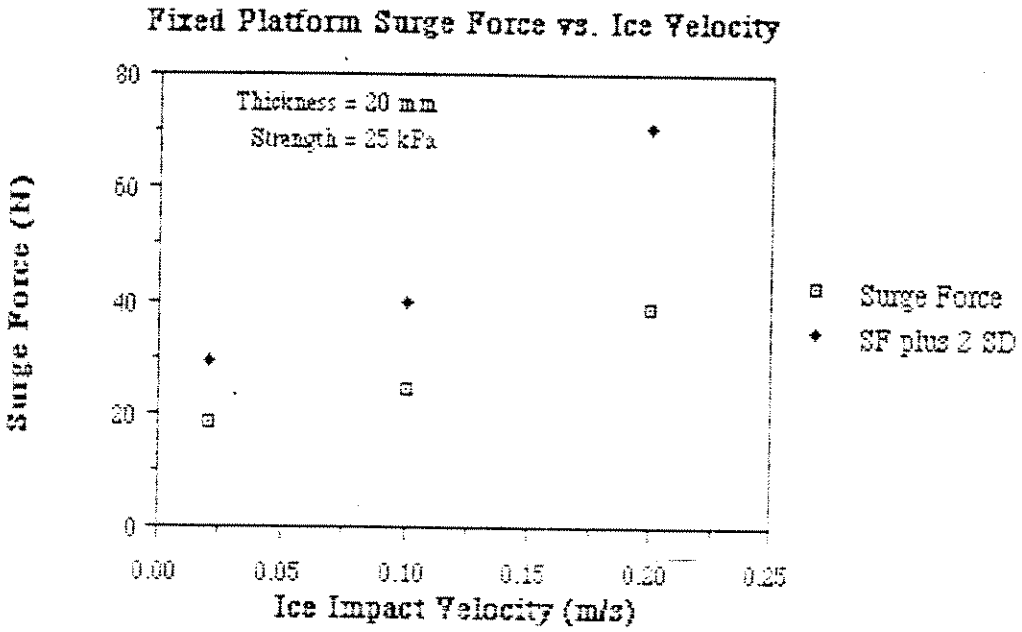

Figure 14. Fixed Platform, Horizontal Force vs. Ice Velocity, Thickness = 20mm, Strength = 25kPa

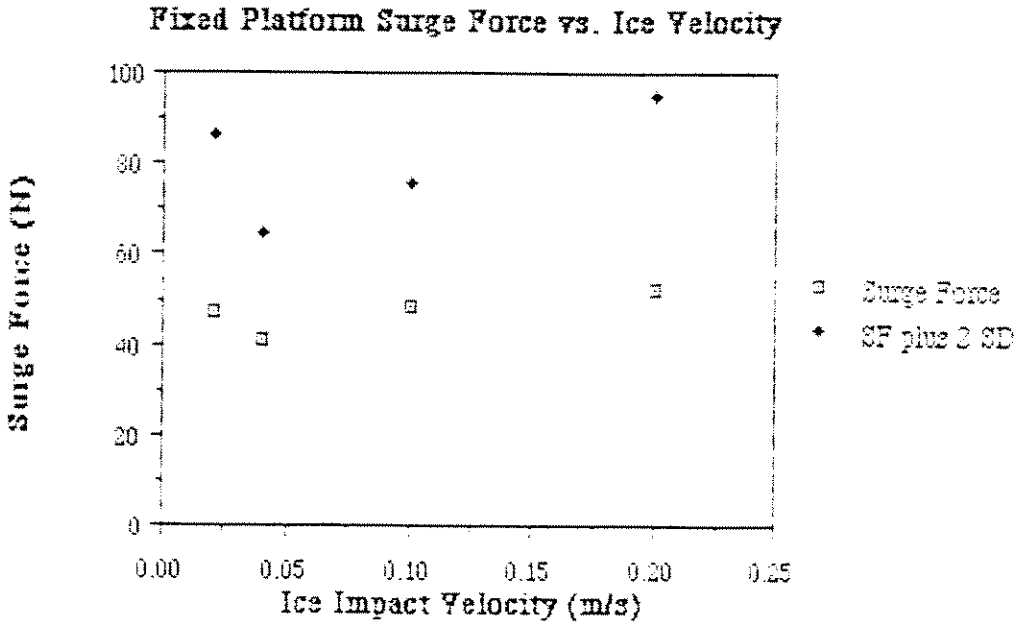

Figure 15. Fixed Platform, Horizontal Force vs. Ice Velocity, Thickness = 30mm, Strength = 25kPa

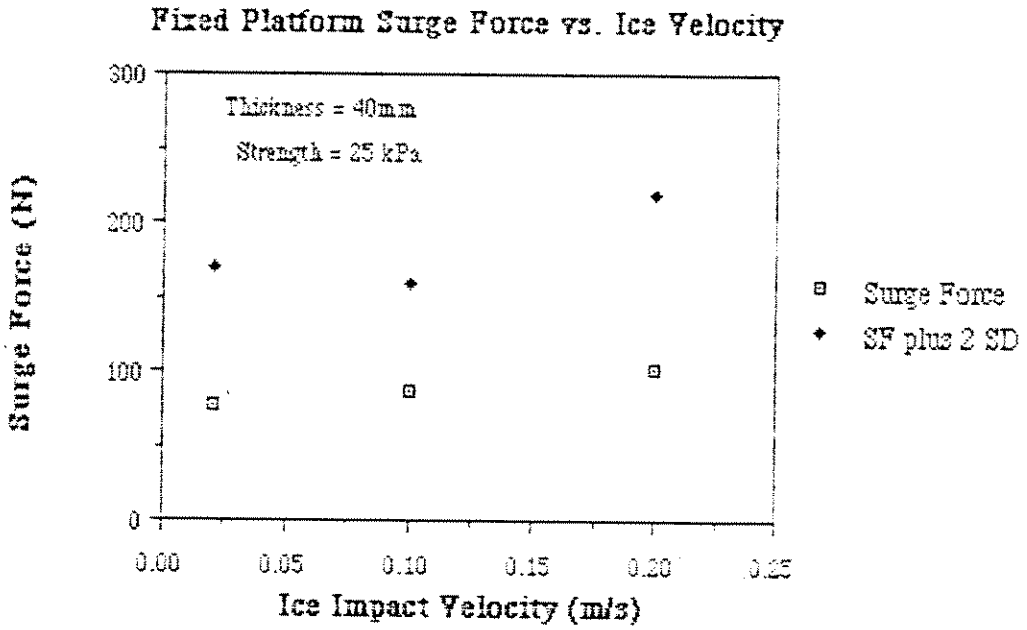

Figure 16. Fixed Platform, Horizontal Force vs. Ice Velocity, Thickness = 40mm, Strength = 25kPa

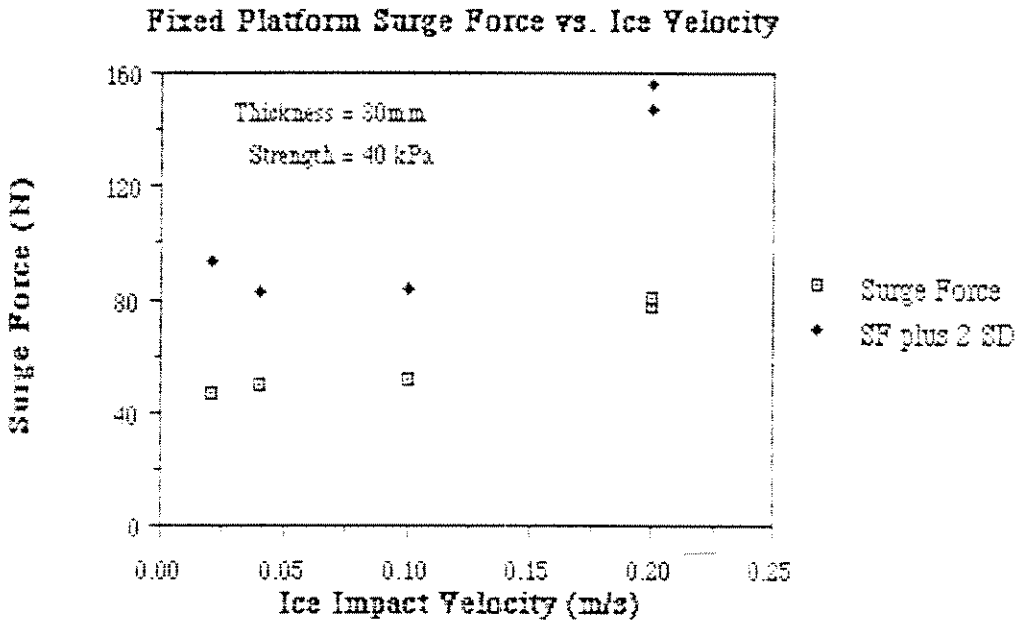

Figure 17. Fixed Platform, Horizontal Force vs. Ice Velocity
Thickness = 30mm, Strength = 40kPa

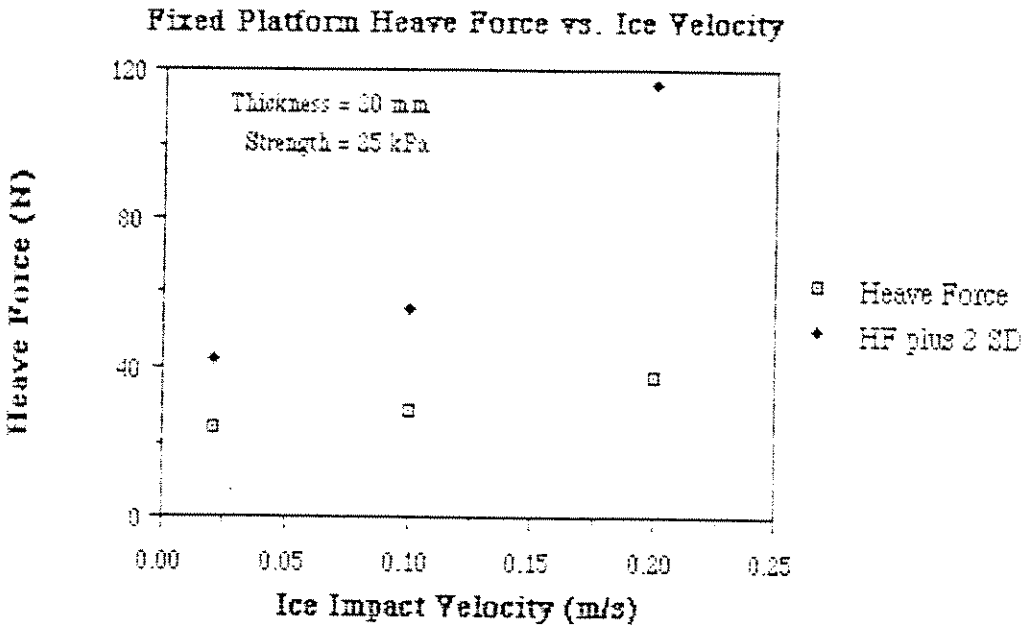

Figure 18. Fixed Platform, Vertical Force vs Ice Velocity, Thickness = 20mm, Strength = 25kPa

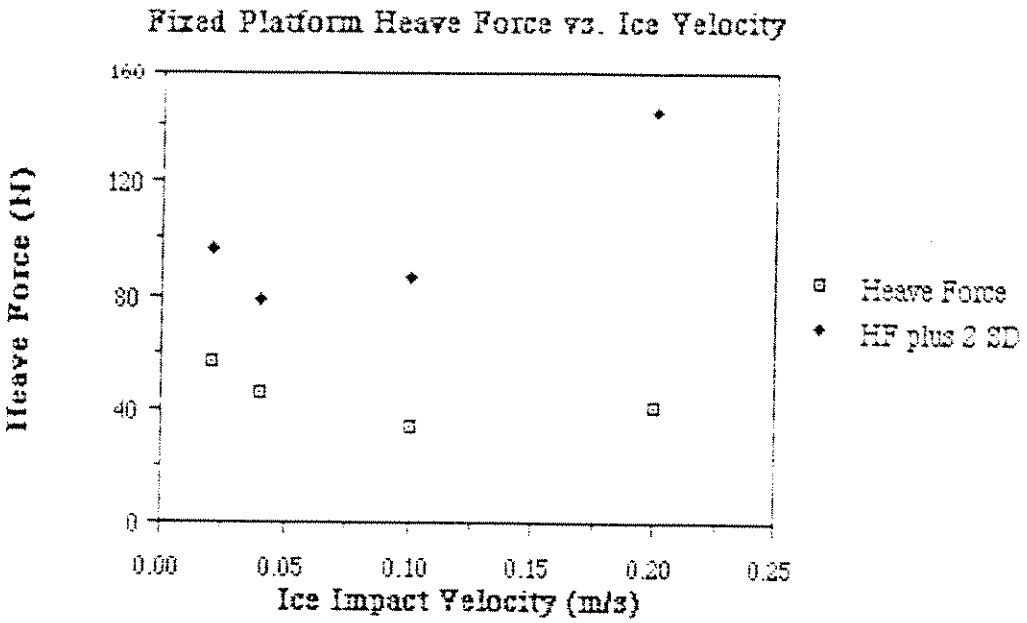

Figure 19. Fixed Platform, Vertical Force vs Ice Velocity, Thickness = 30mm, Strength = 25kPa

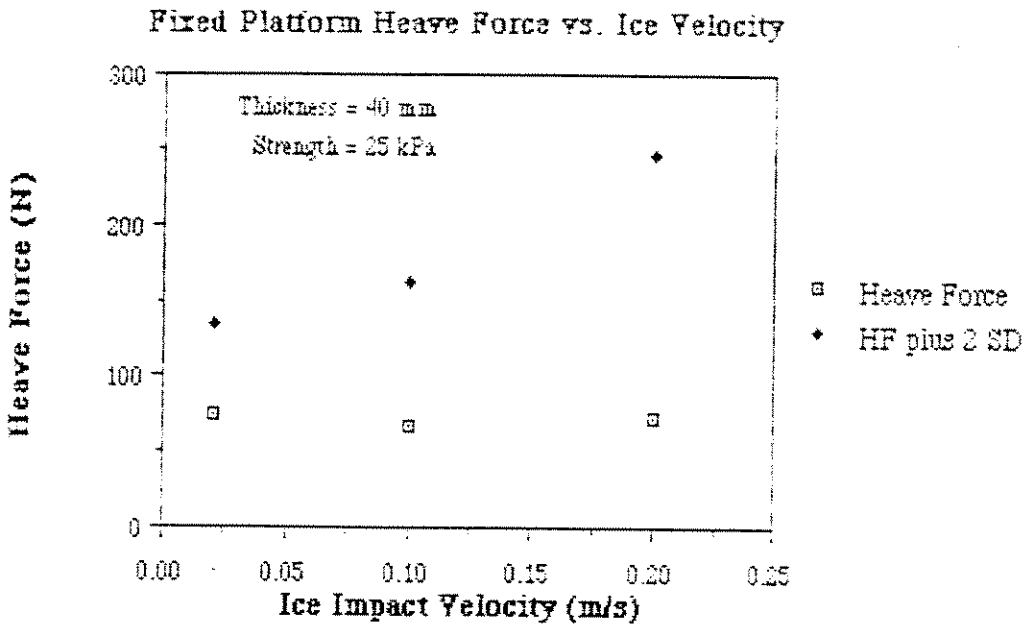

Figure 20. Fixed Platform, Vertical Force vs Ice Velocity, Thickness = 40mm, Strength = 25kPa

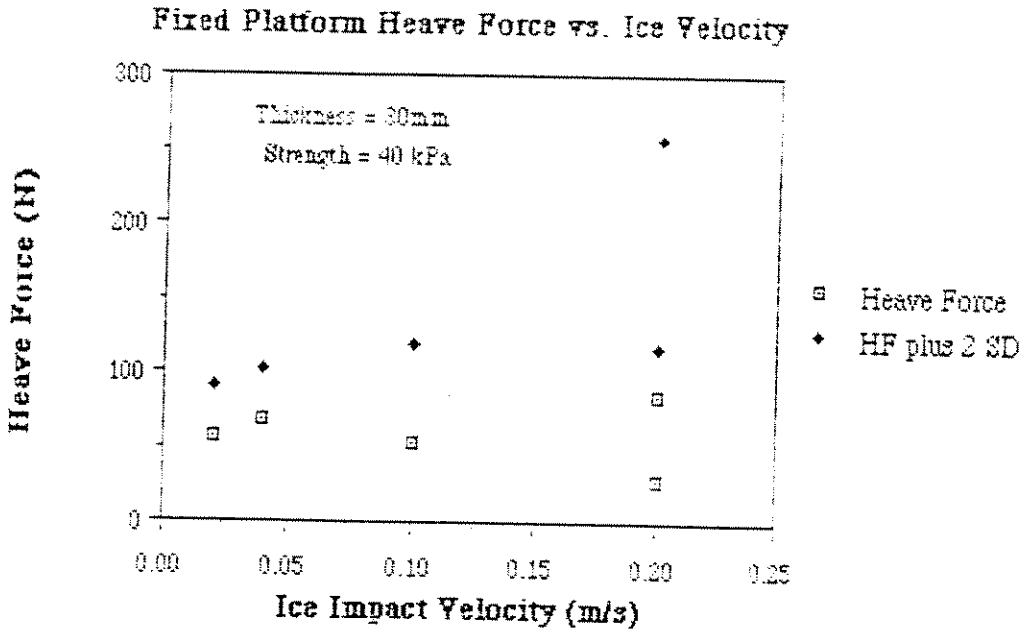

Figure 21. Fixed Platform, Vertical Force vs Ice Velocity, Thickness = 30mm. Strength = 40kPa

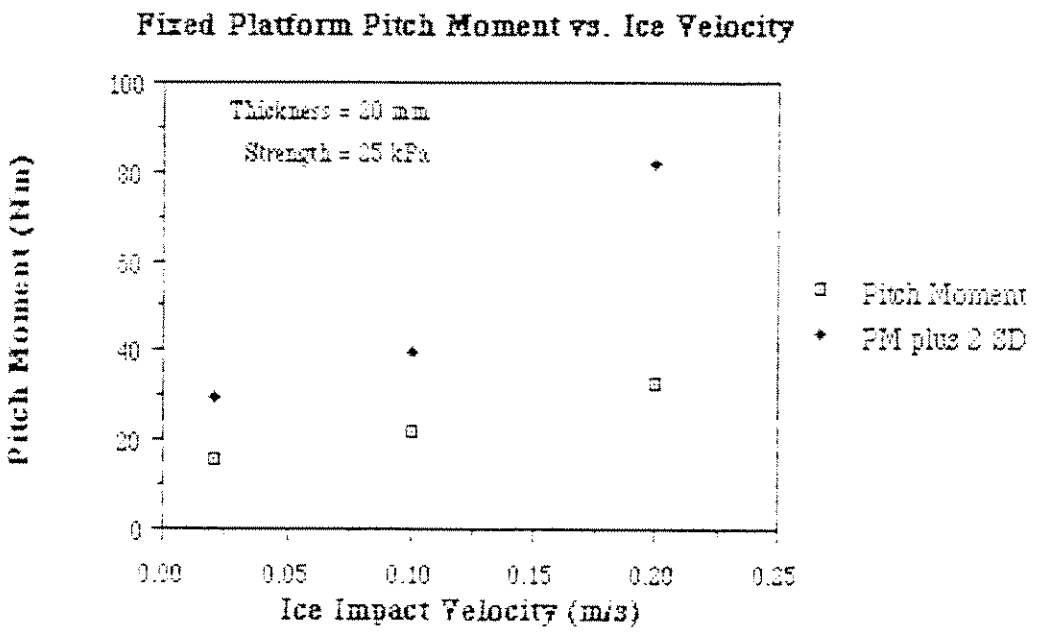

Figure 22. Fixed Platform, Pitch Moments vs Ice Velocity, Thickness = 20mm, Strength = 25kPa

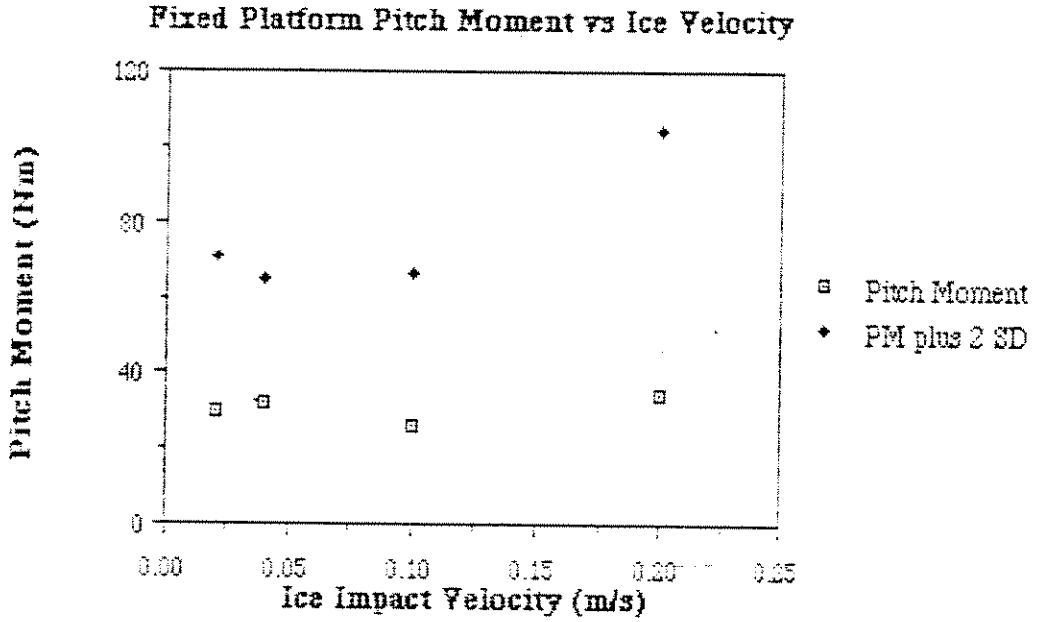

Figure 23. Fixed Platform, Pitch Moments vs Ice Velocity, Thickness = 30mm, Strength = 25kPa

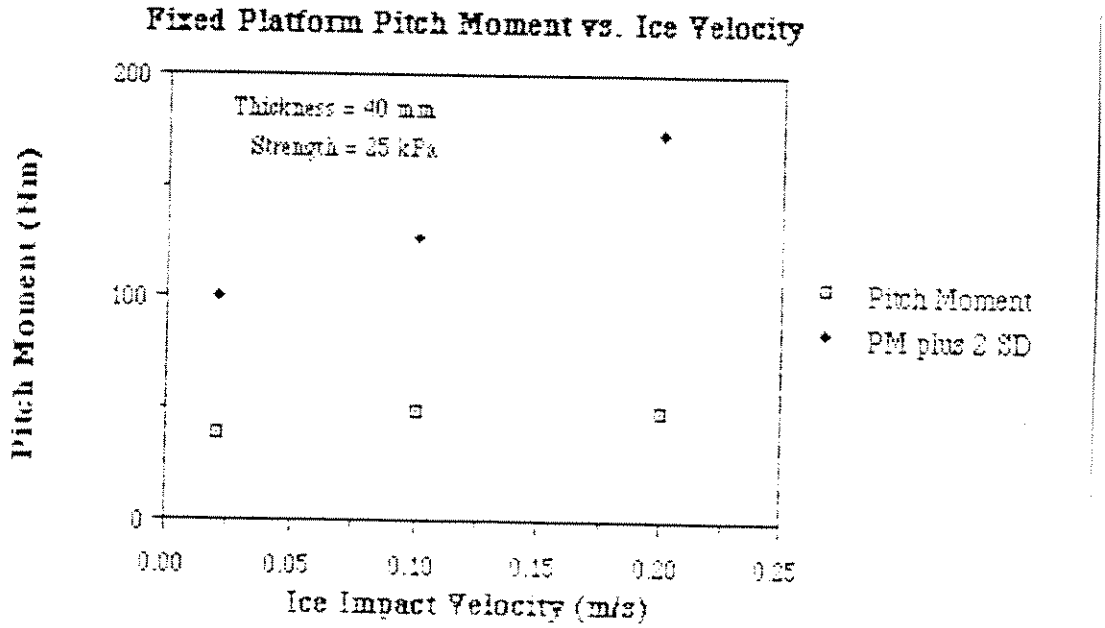

Figure 24. Fixed Platform, Pitch Moments vs Ice Velocity, Thickness = 40mm, Strength = 25kPa

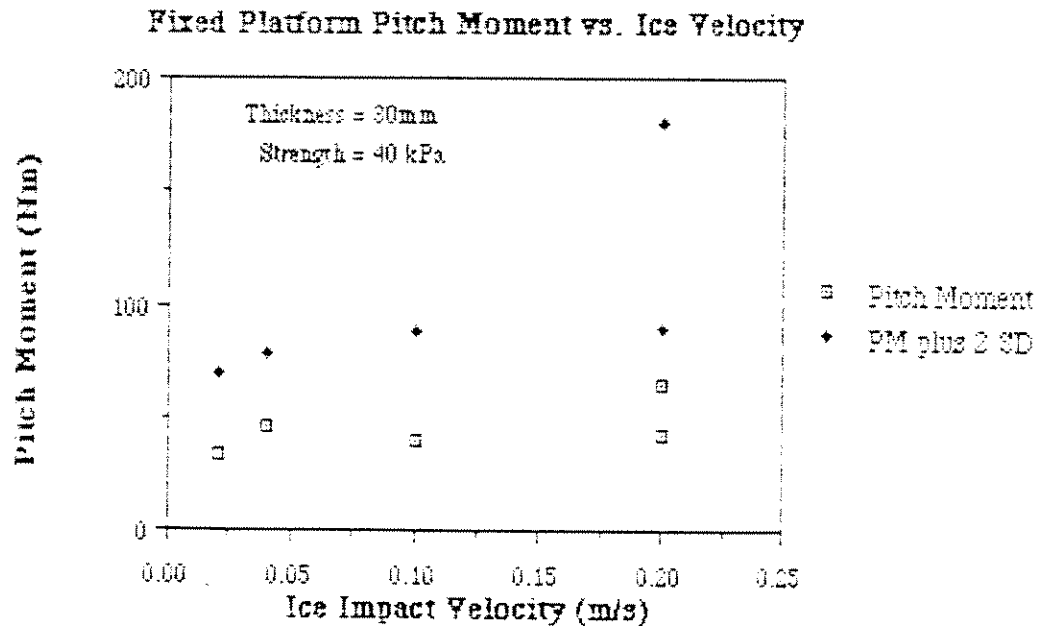

Figure 25. Fixed Platform, Pitch Moments vs Ice Velocity, Thickness = 30mm, Strength = 40kPa

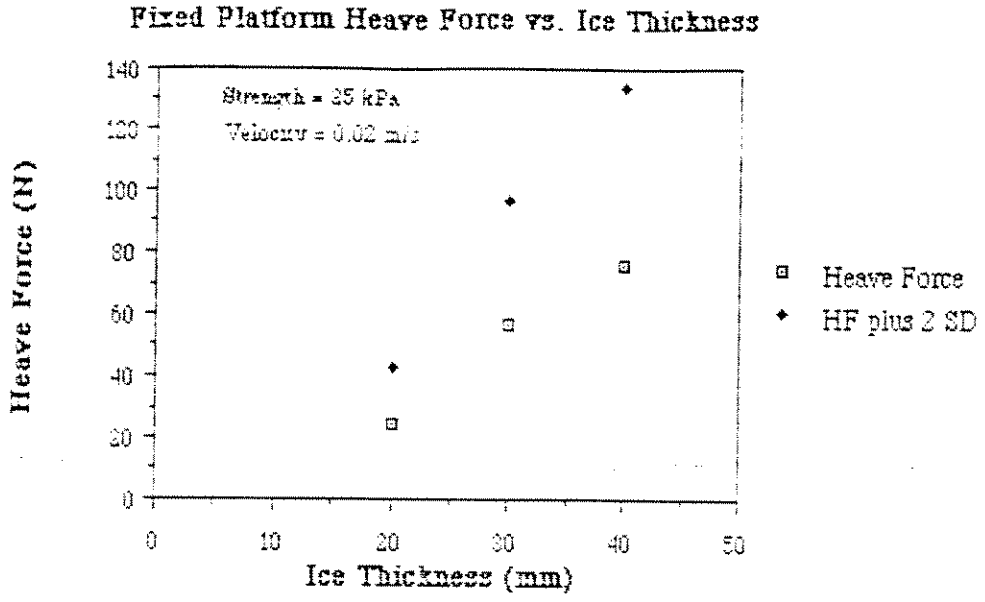

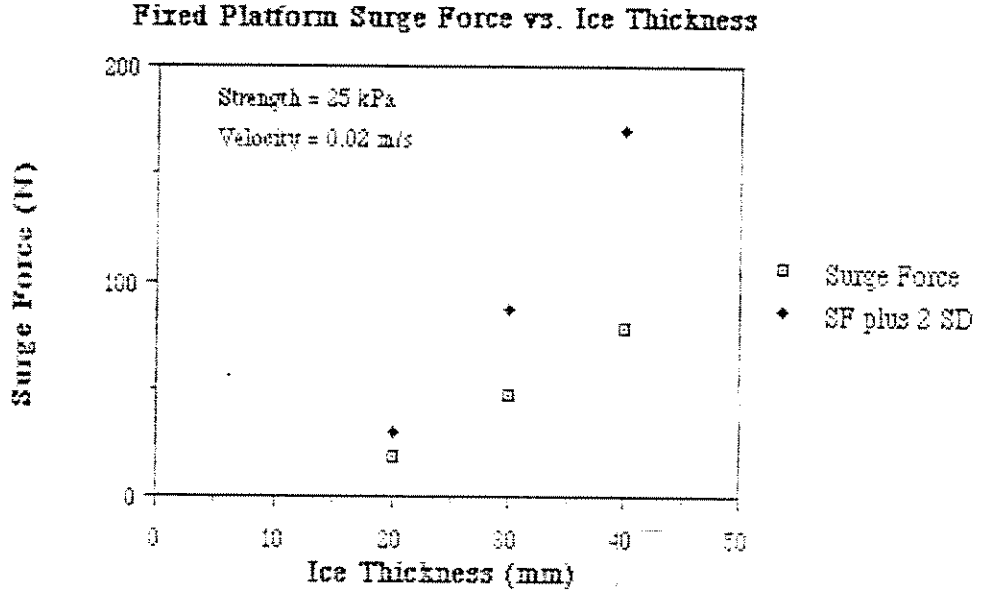

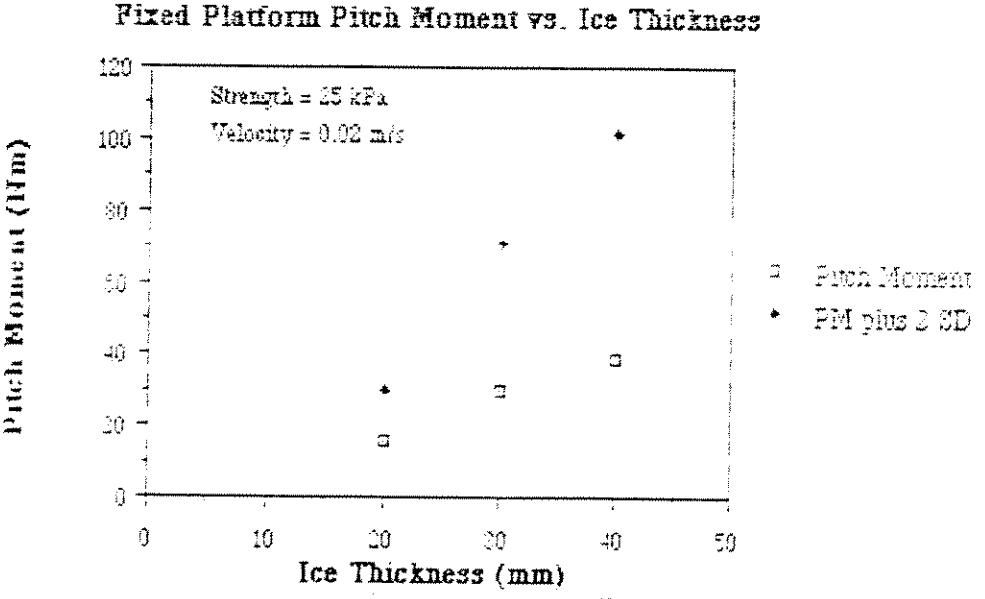

Figure 26. Forces and Moments vs Ice Thickness, Velocity = 0.02m/s, Strength = 25kPa

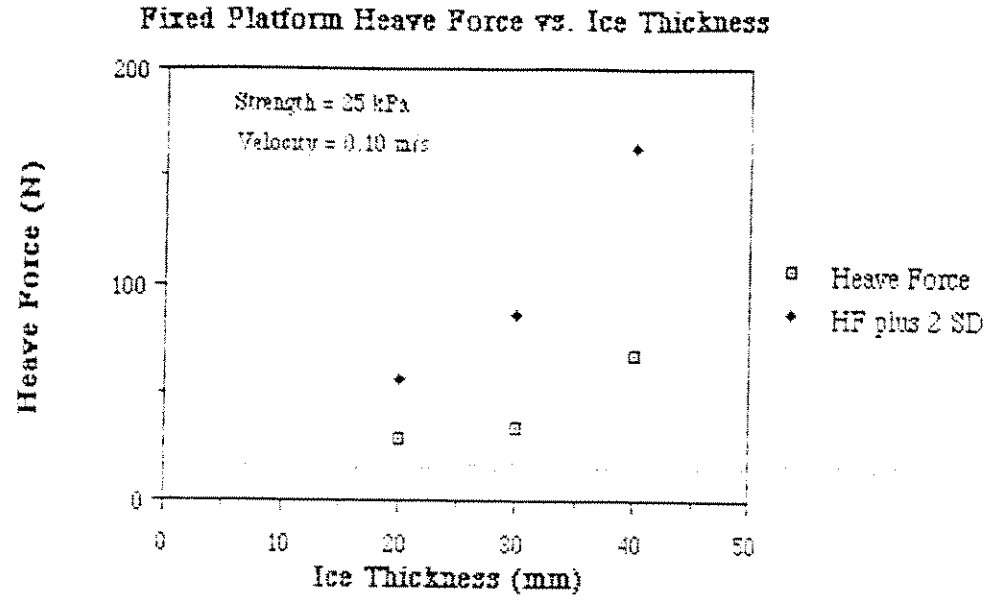

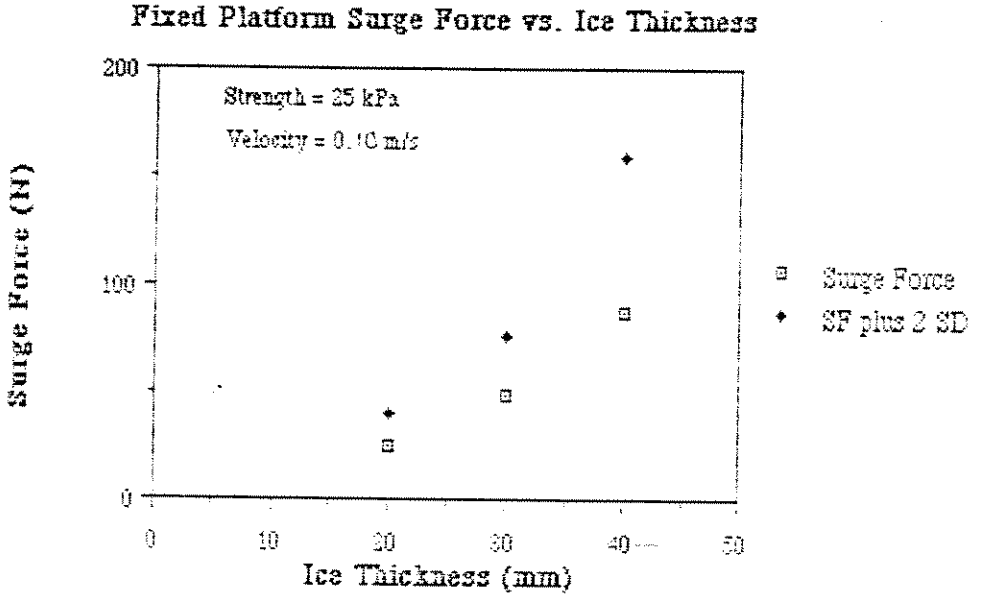

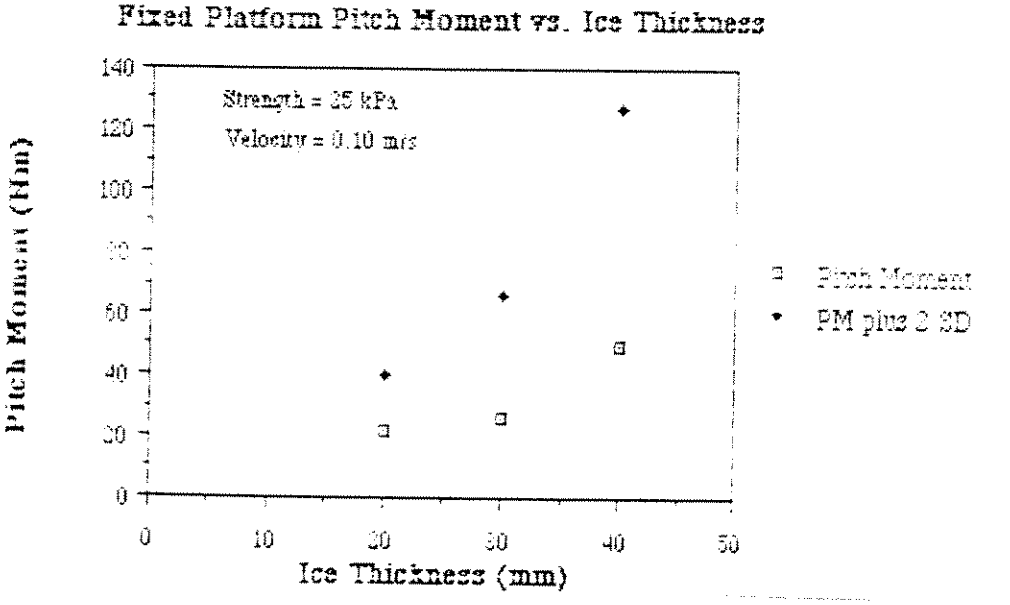

Figure 27. Forces and Moments vs Ice Thickness,

Velocity = 0.10m/s, Strength = 25kPa

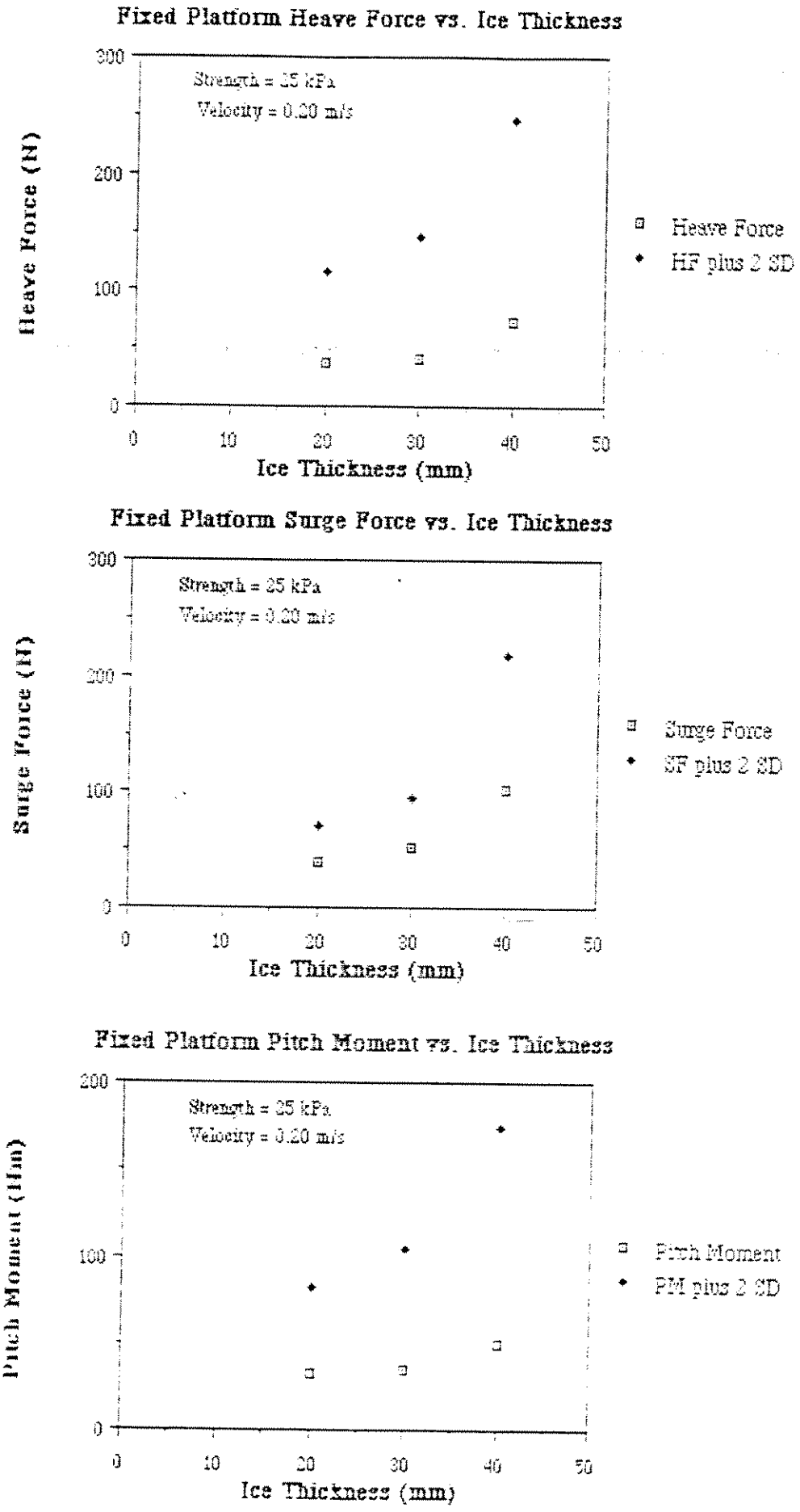

Figure 28. Forces and Moments vs Ice Thickness, Velocity = 0.20m/s, Strength = 25kPa

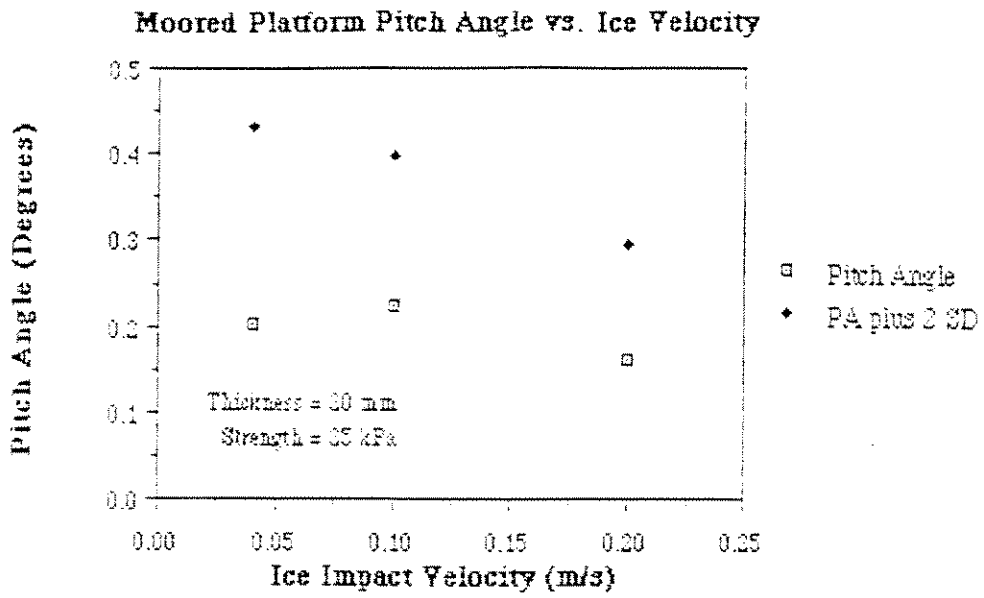

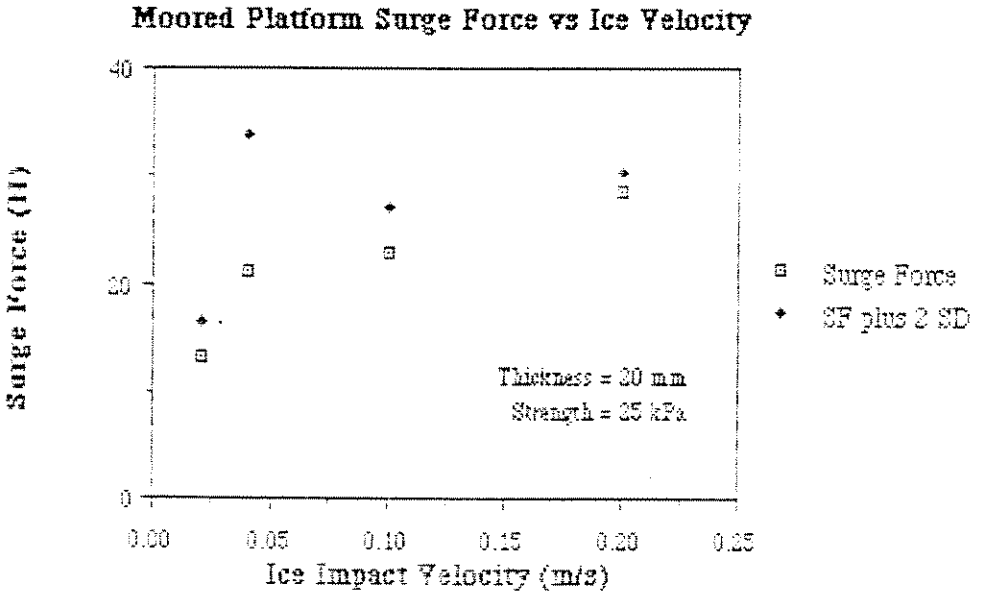

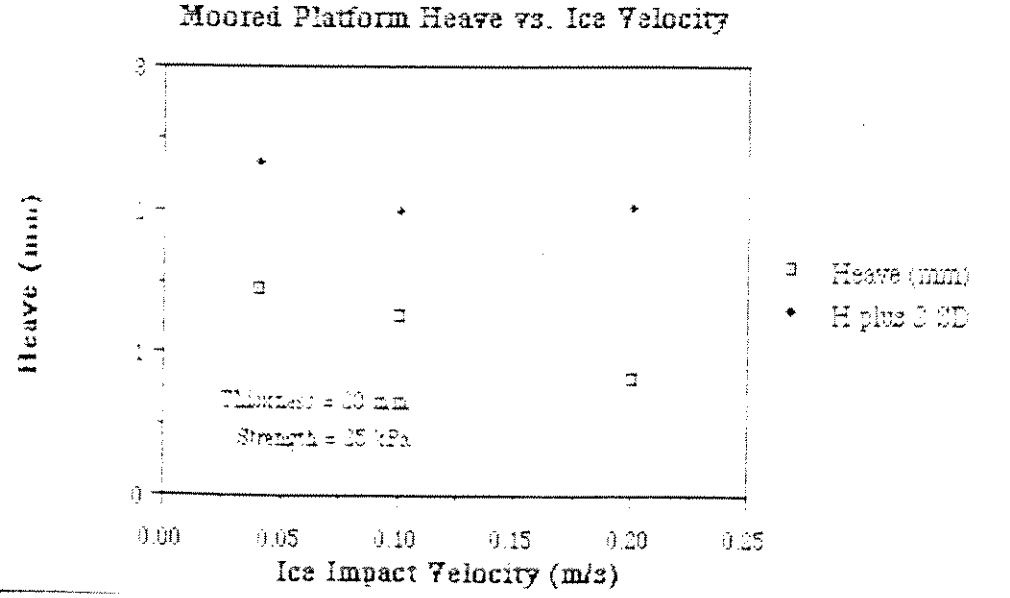

Figure 29. Moored Platform: Horizontal Force vs Ice Velocity, Thickness = 20mm, Strength = 25kPa

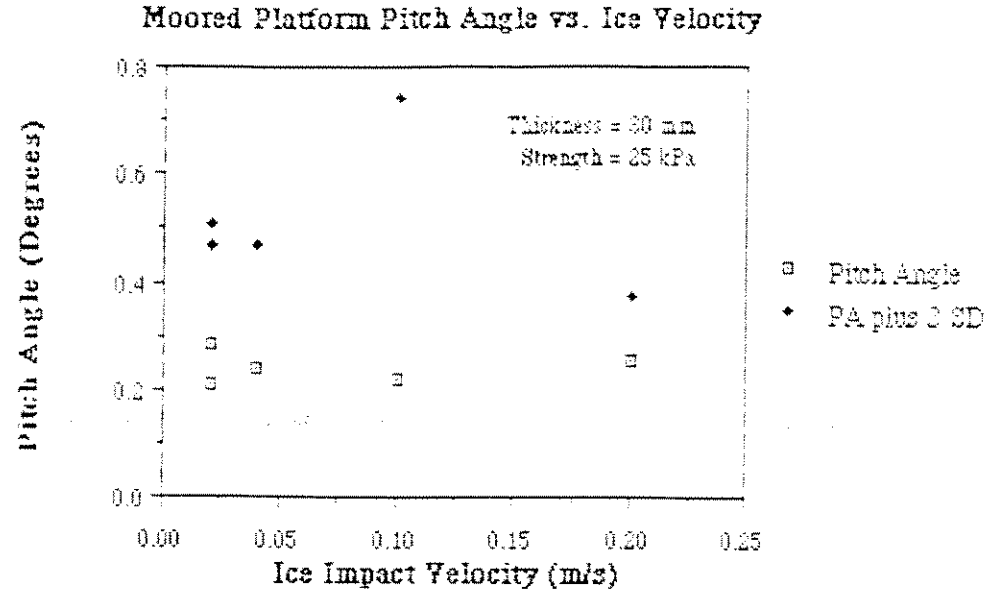

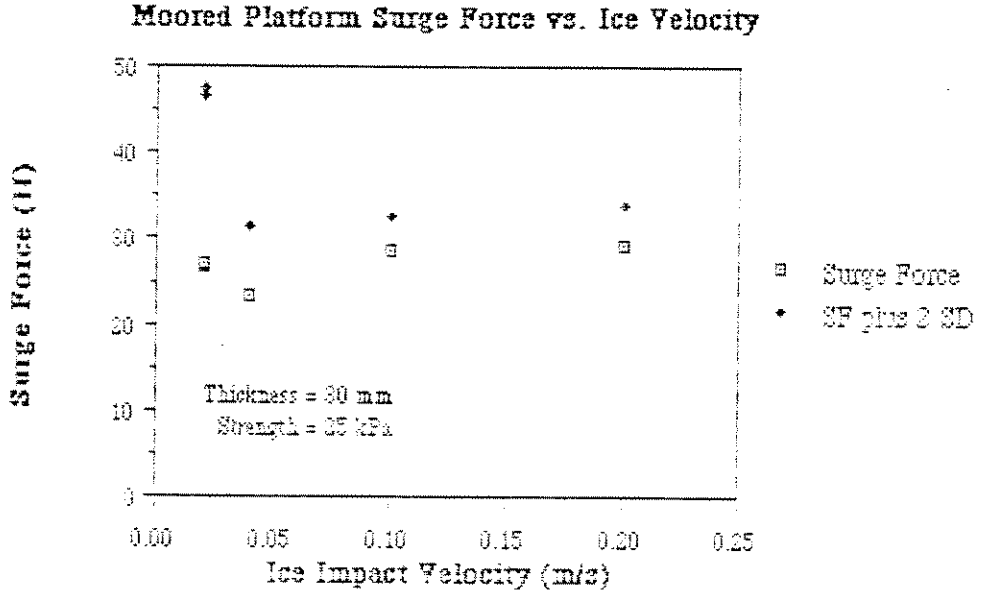

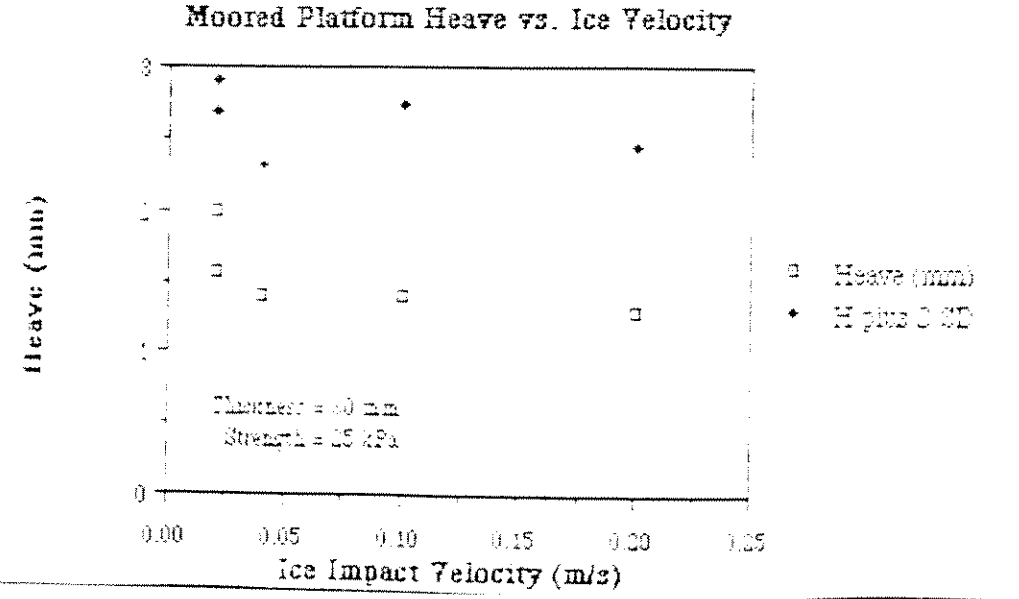

Figure 30. Moored Platform: Horizontal Force vs Ice Velocity, Thickness = 30mm, Strength = 25kPa

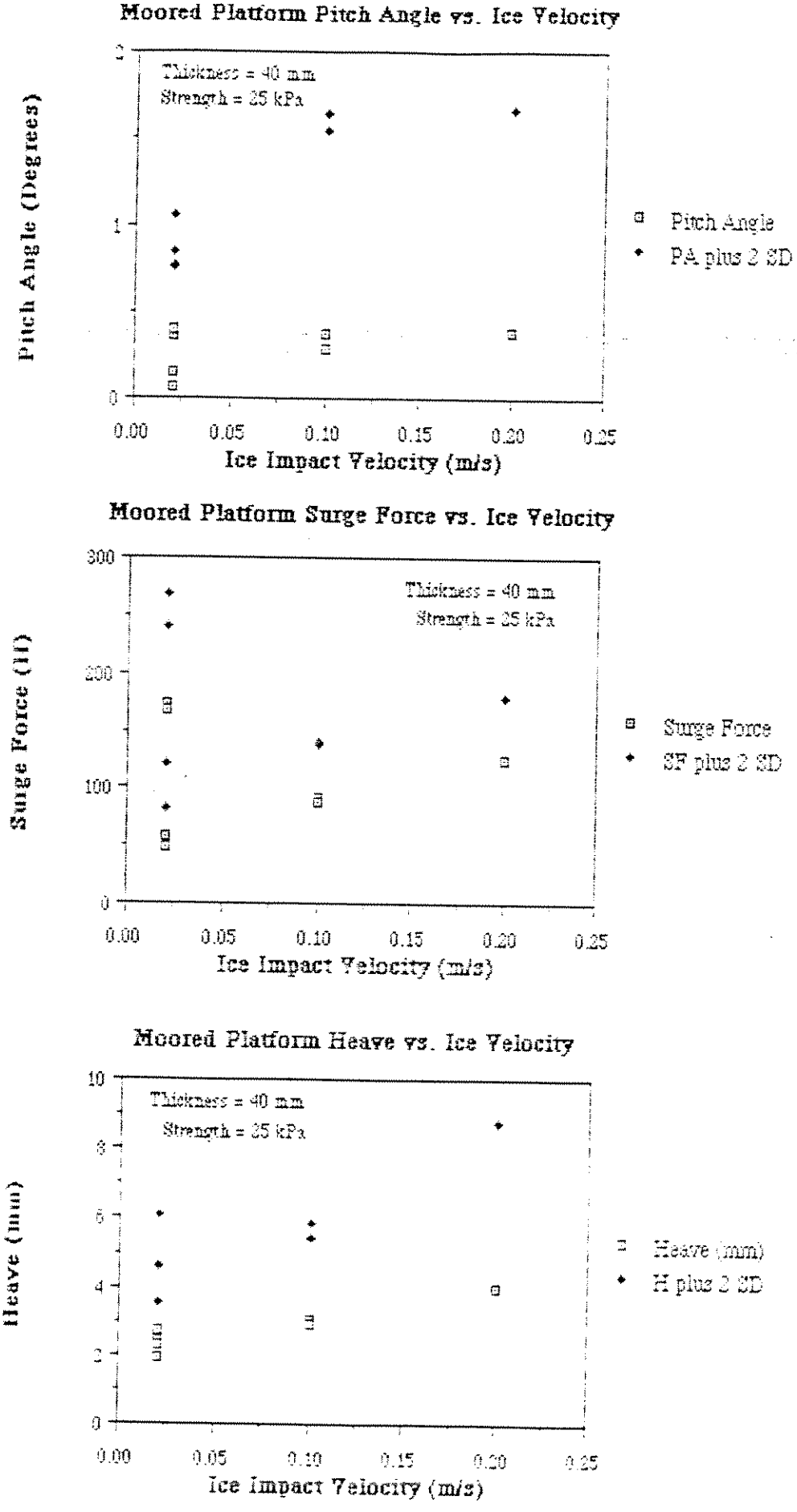

Figure 31. Moored Platform: Horizontal Force vs Ice Velocity, Thickness = 40mm, Strength = 25kPa

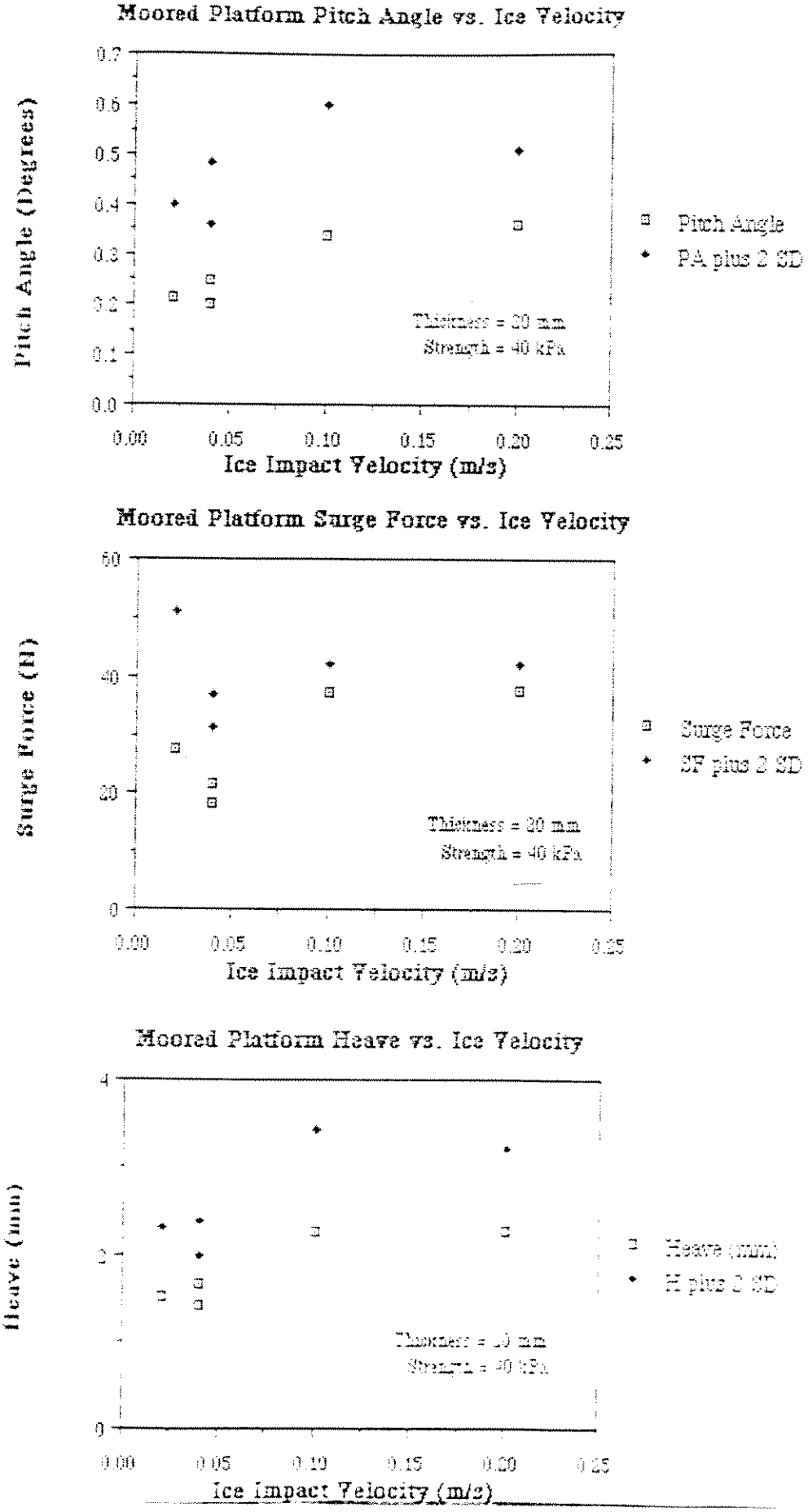

Figure 32. Moored Platform: Horizontal Force vs Ice Velocity,

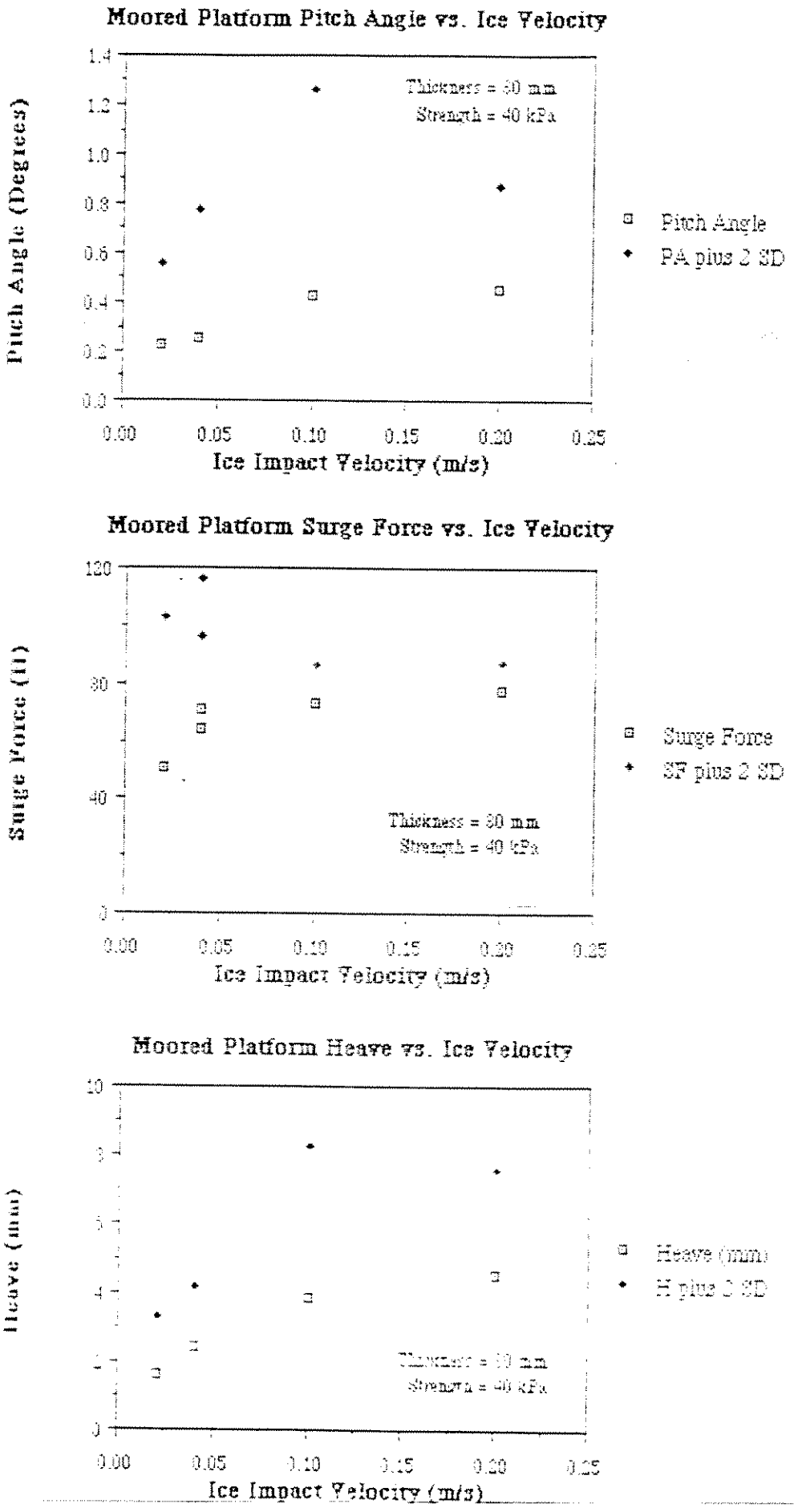

Figure 33. Moored Platform: Horizontal Force vs Ice Velocity,

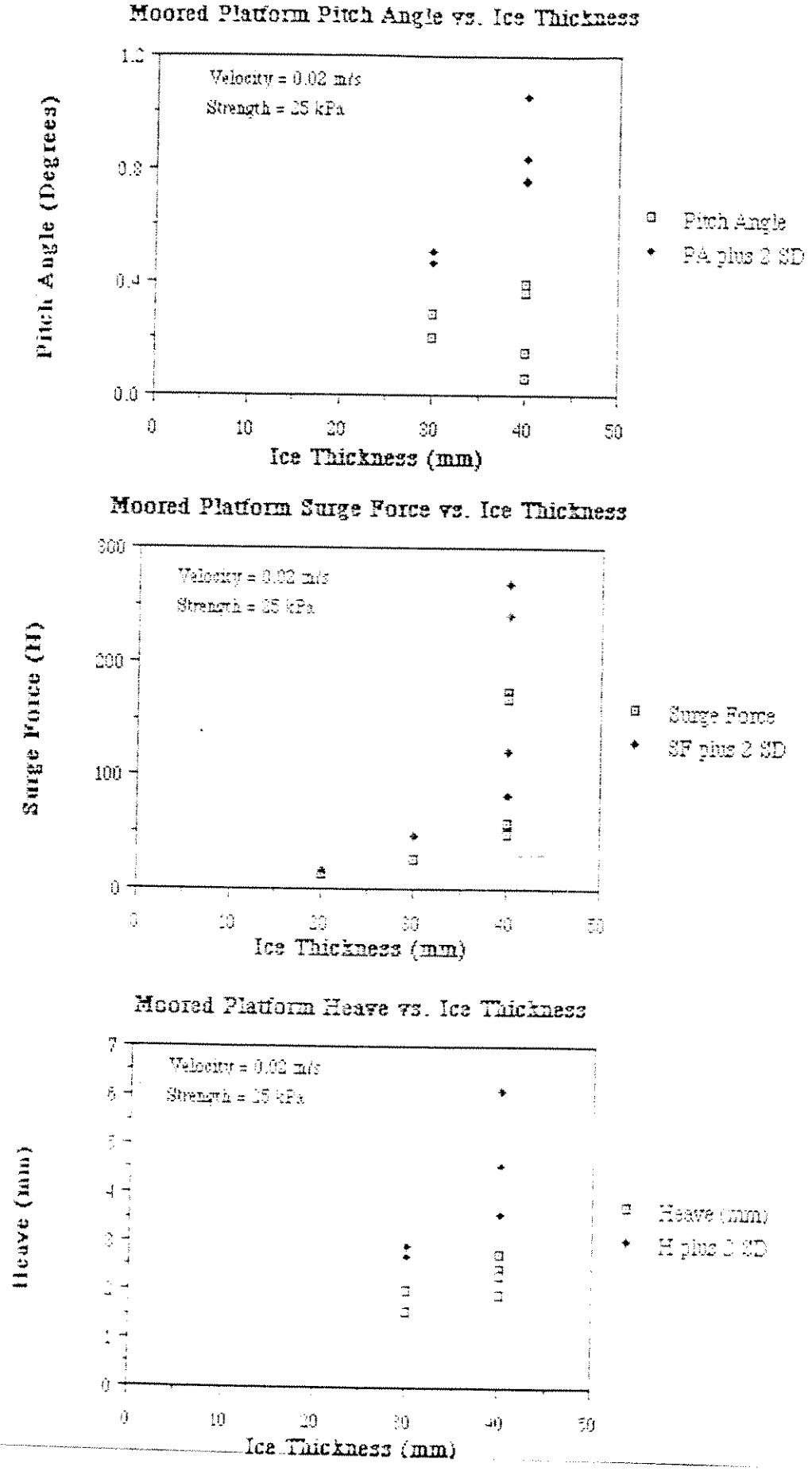

Figure 34. Moored Platform: Horizontal Force vs Ice Thickness, Velocity = 0.02m/s, Strength = 25kPa

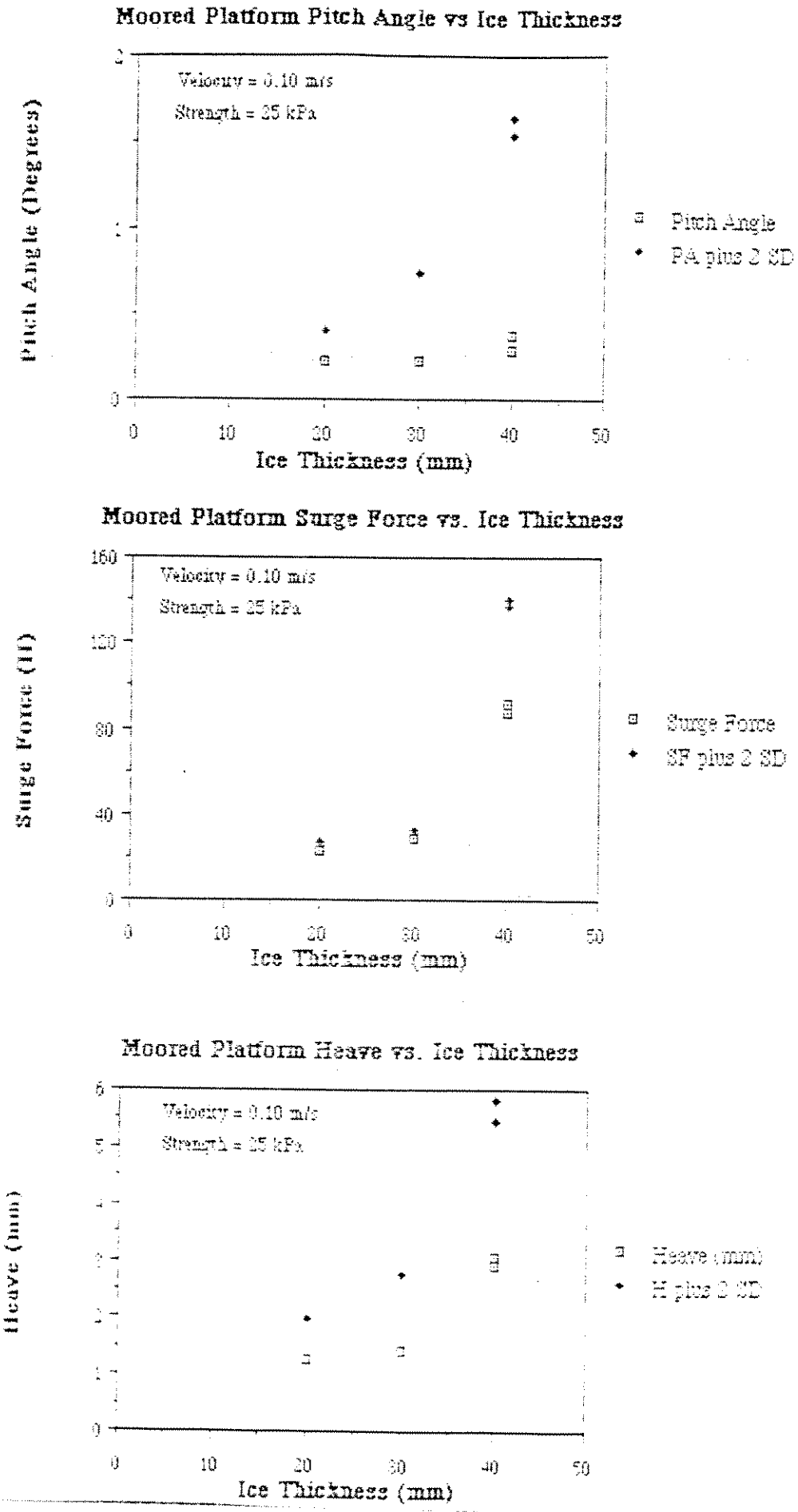

Figure 35. Moored Platform: Horizontal Force vs Ice Thickness, Velocity = 0.10m/s, Strength = 25kPa

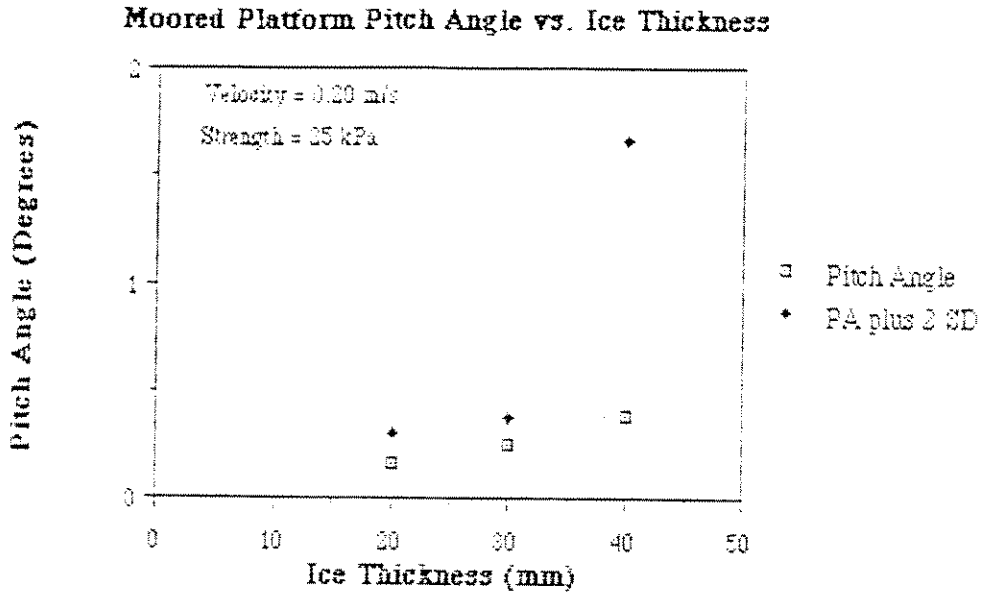

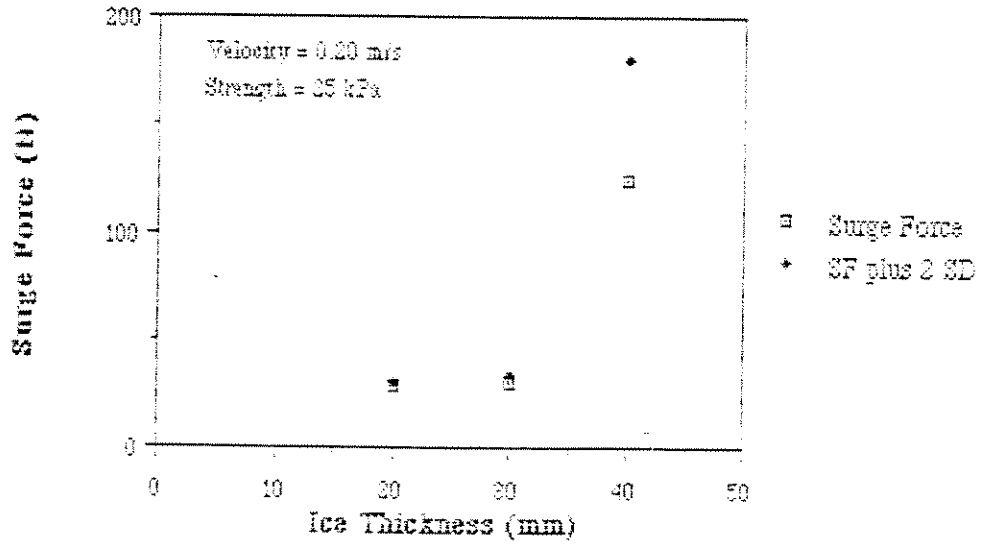

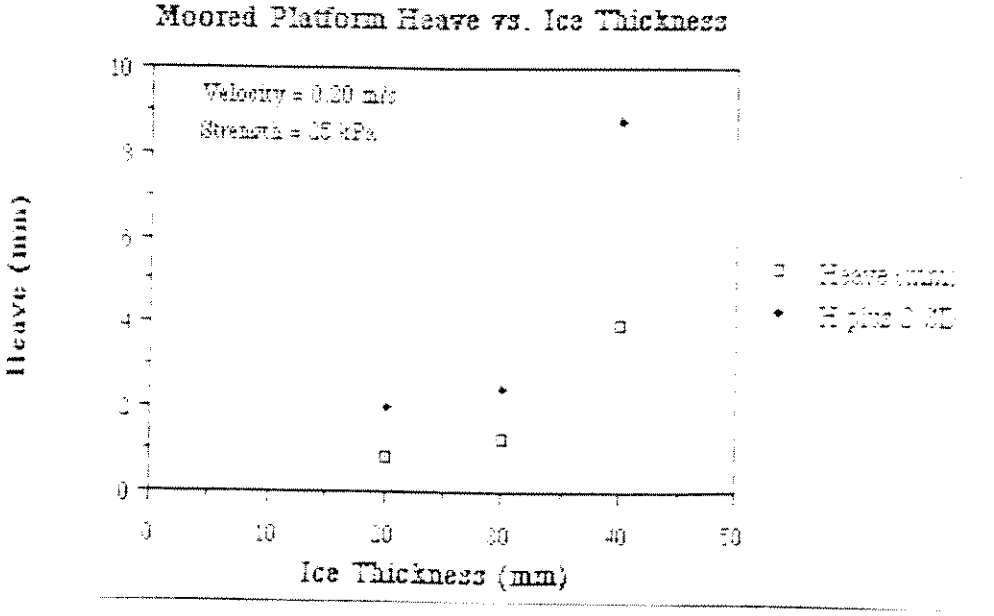

Figure 36. Moored Platform: Horizontal Force vs Ice Thickness, Velocity = 0.20m/s Strength = 25kPa

Figure 37. Ice Trapped Underneath the Platform, Shown after the Test

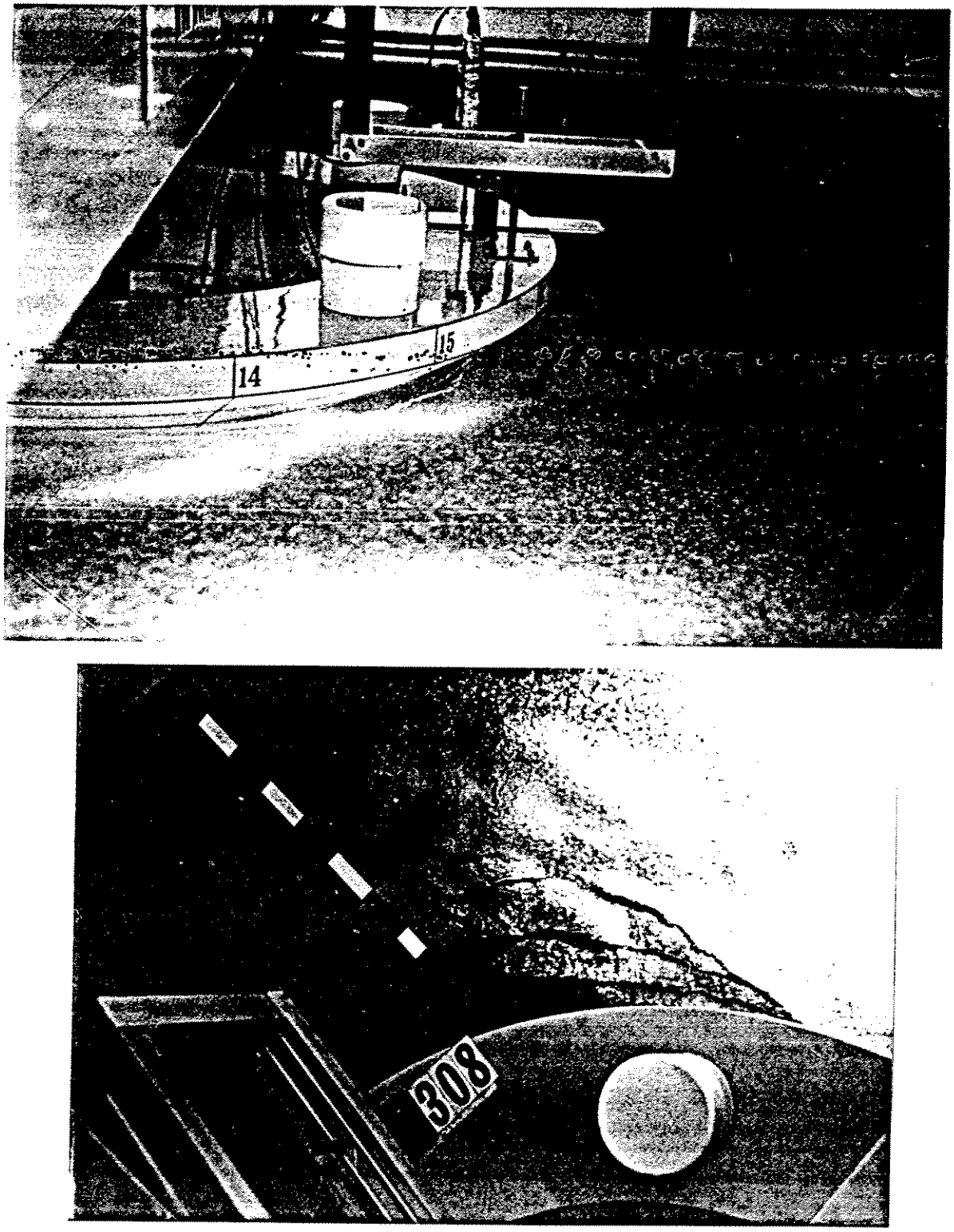

Figure 38. Circumferential Ice Fracture Around Platform

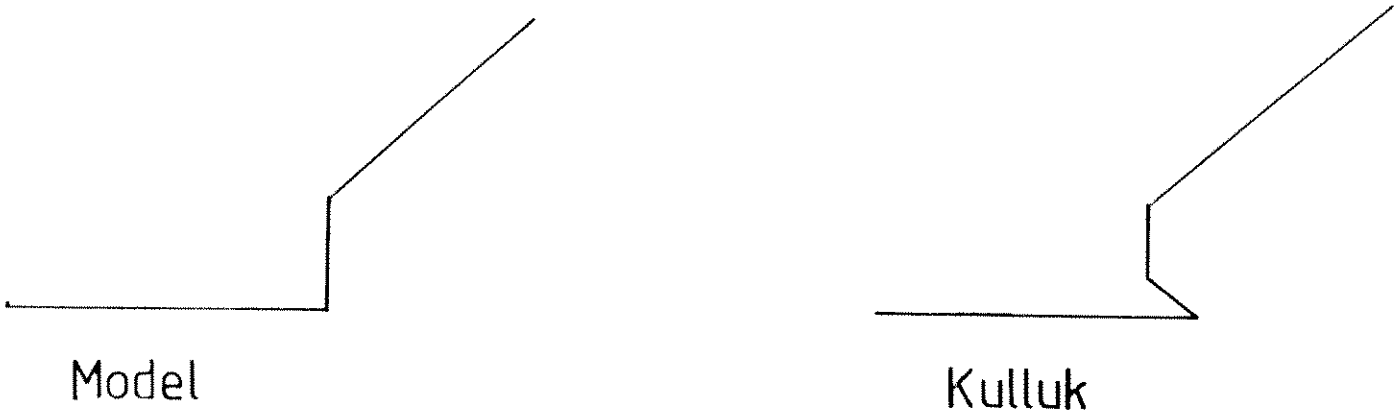

Figure 39. Comparison of "Skirts" for Model and "Kulluk"

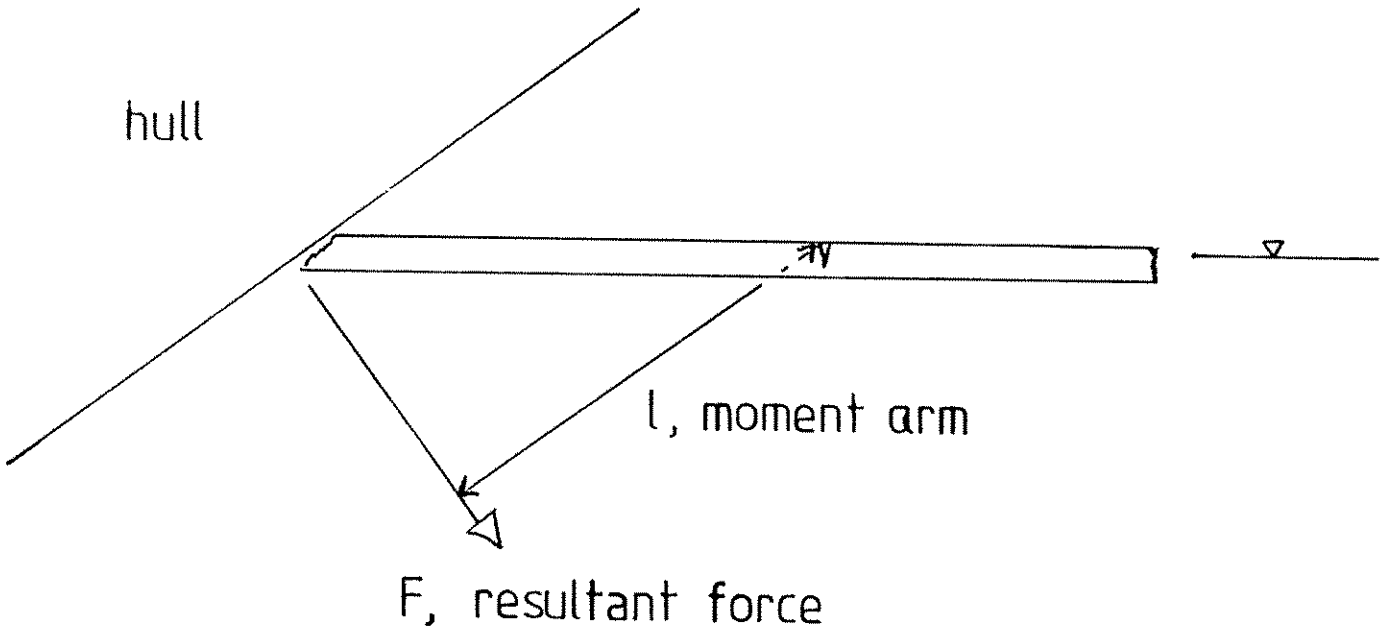

Figure 40. Depiction of Forces Acting on the Ice Sheet

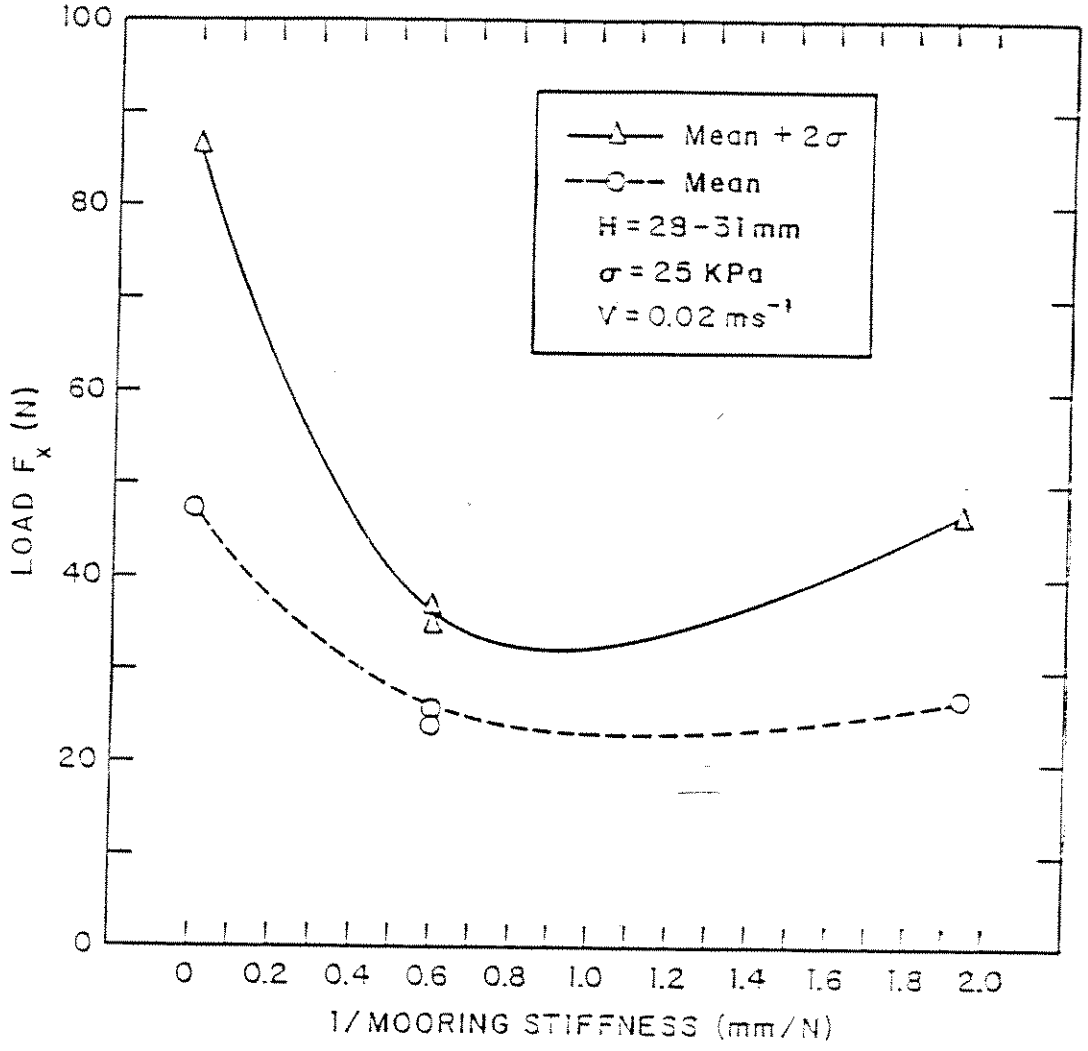

Figure 41. Surge Force vs. $1/K_s$ (Inverse of Mooring Stiffness)

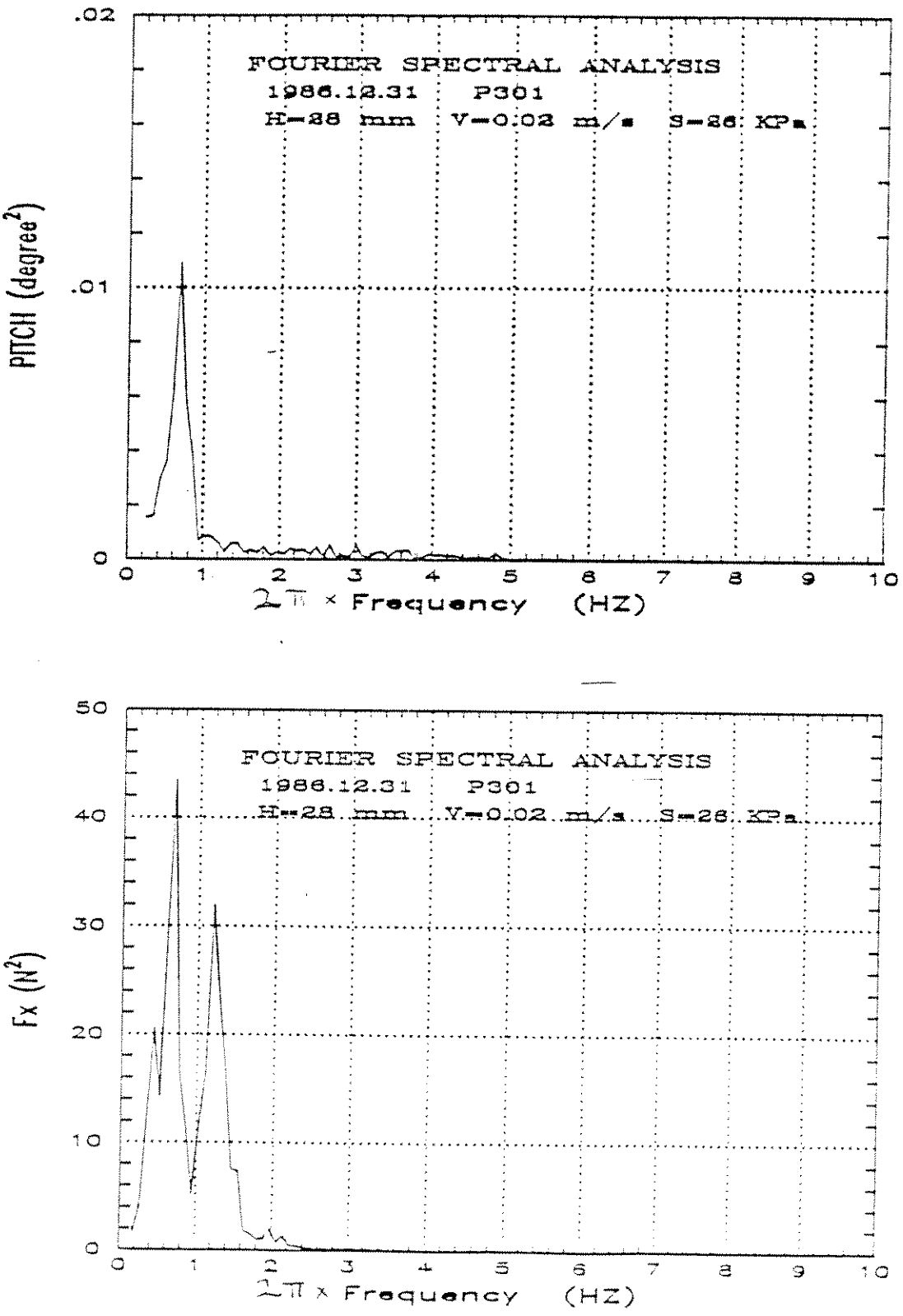

Figure 42. Frequency Power Spectra for Fx and θ, test P301 (moored)

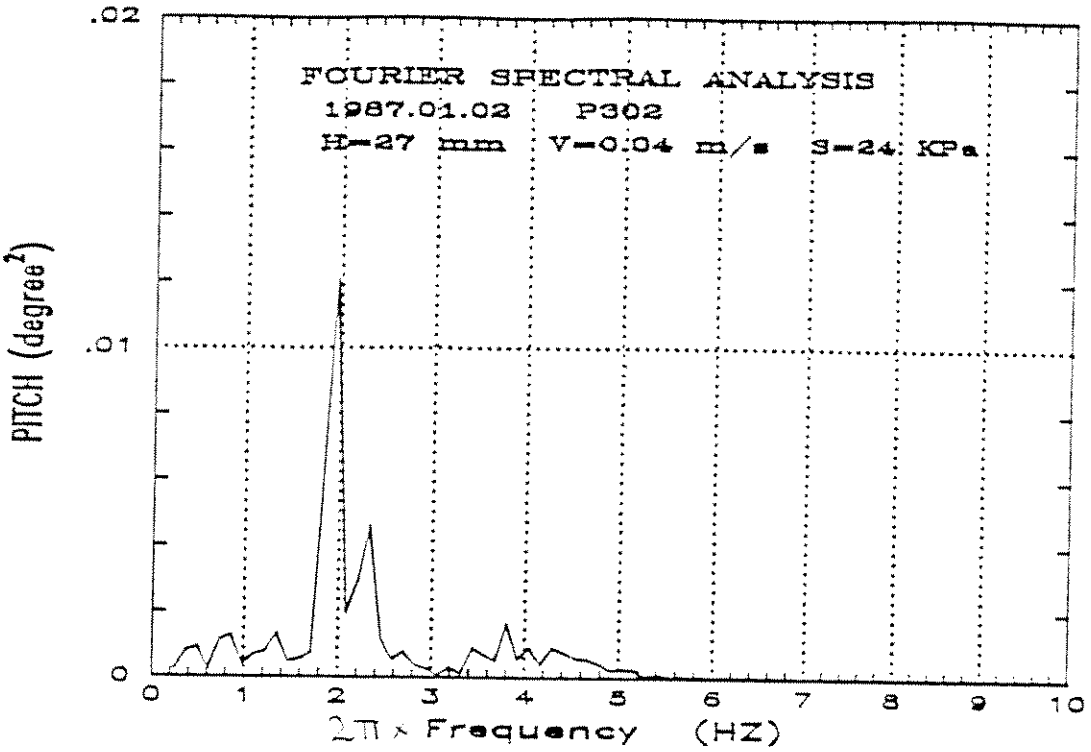

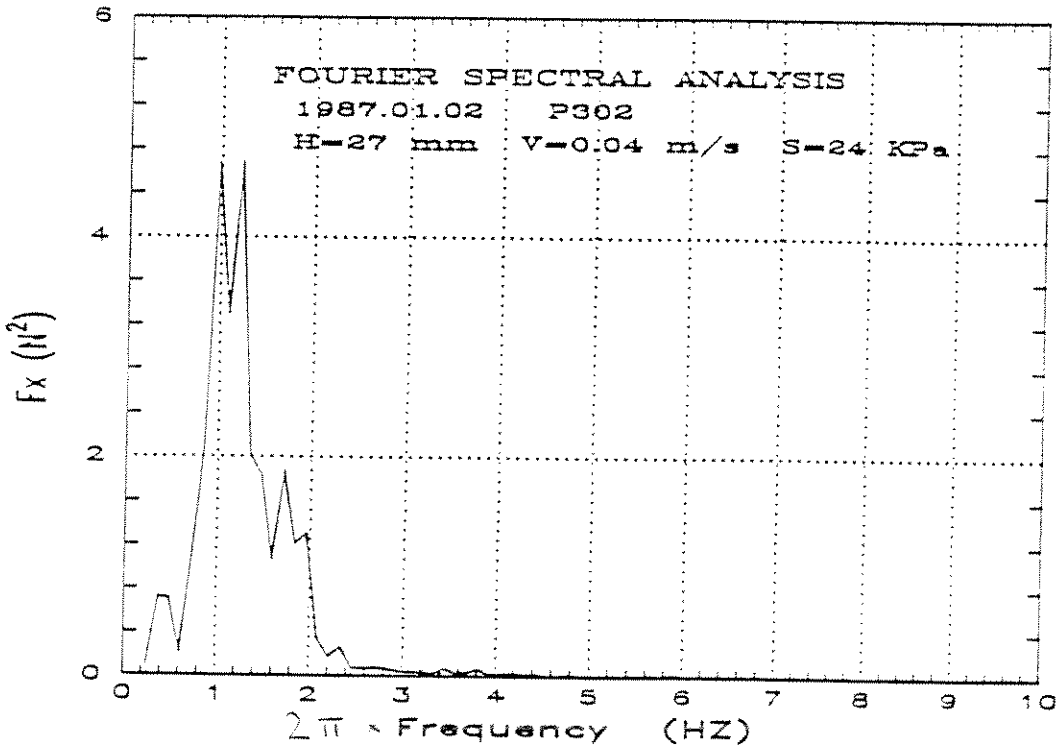

Figure 43. Frequency Power Spectra for Fx and θ, test P302 (moored)

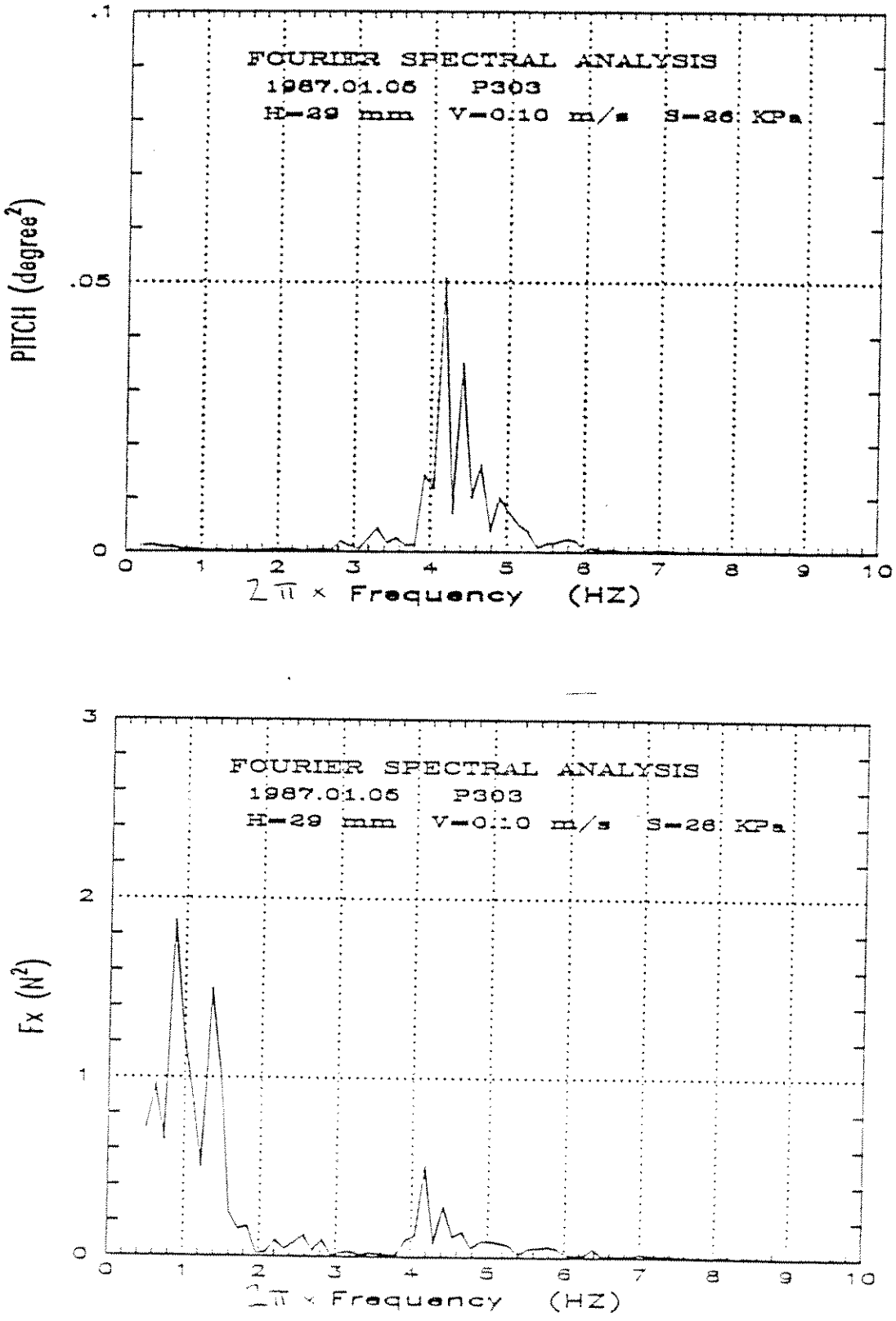

Figure 44. Frequency Power Spectra for Fx and θ, test P303 (moored)

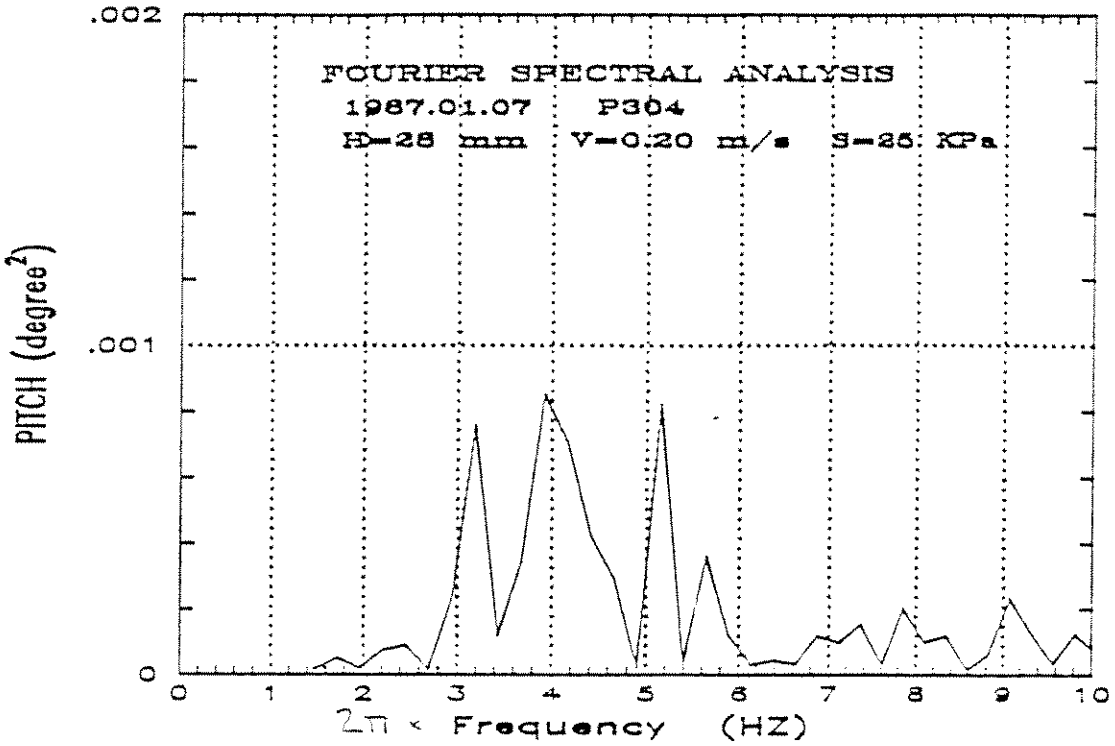

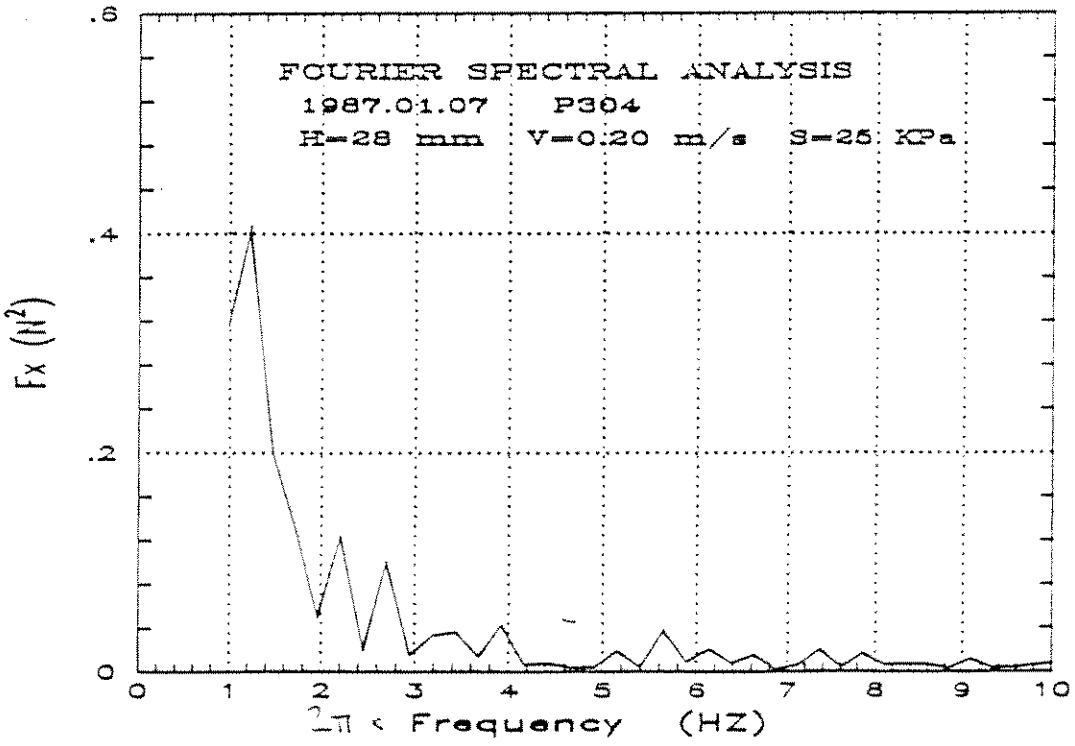

Figure 45. Frequency Power Spectra for Fx and θ, test P304 (moored)

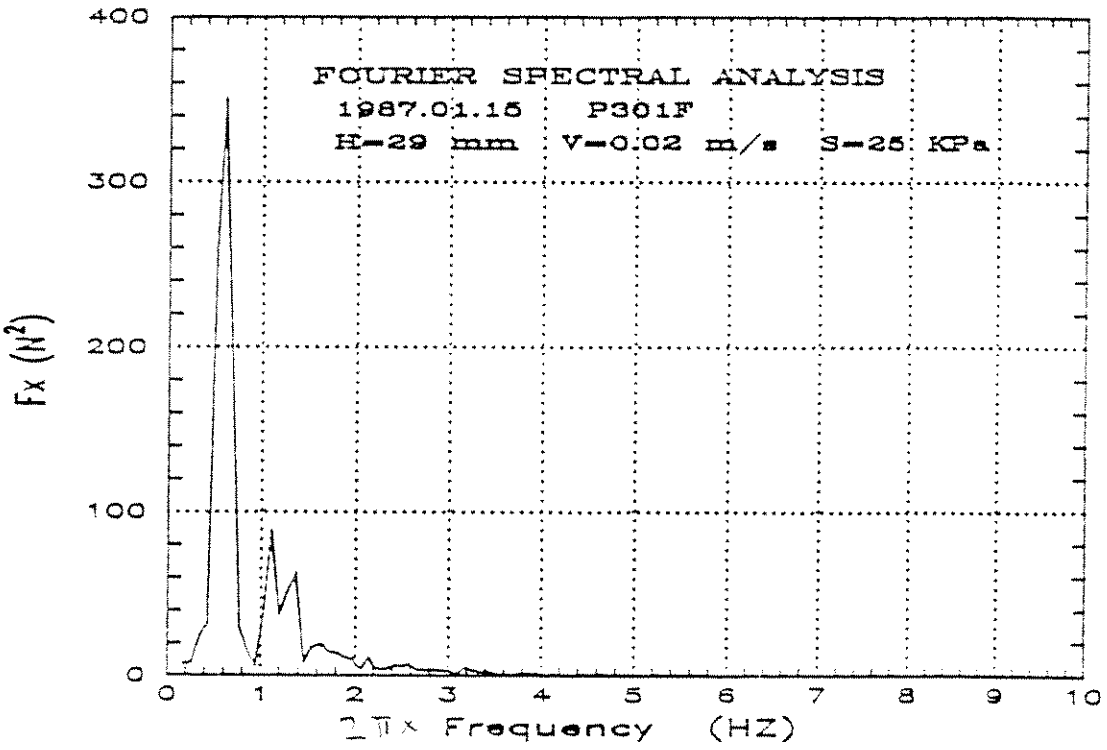

Figure 46. Frequency Power Spectrum for Fx, test P301F (fixed)

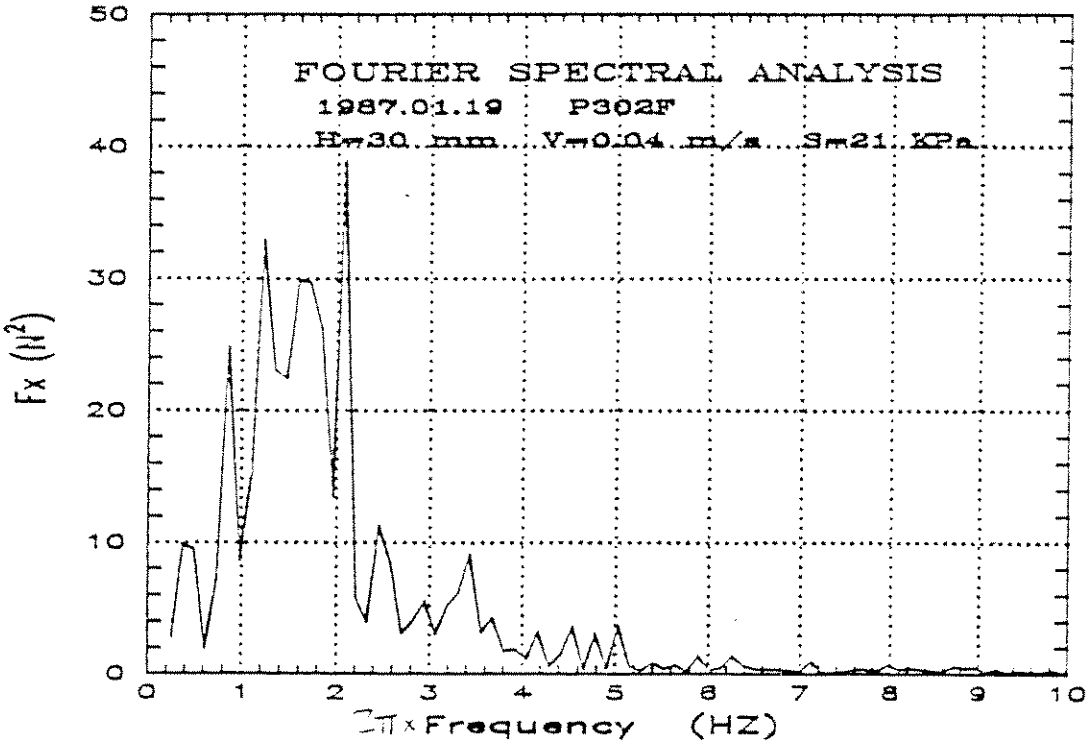

Figure 47. Frequency Power Spectrum for Fx, test P302F (fixed)

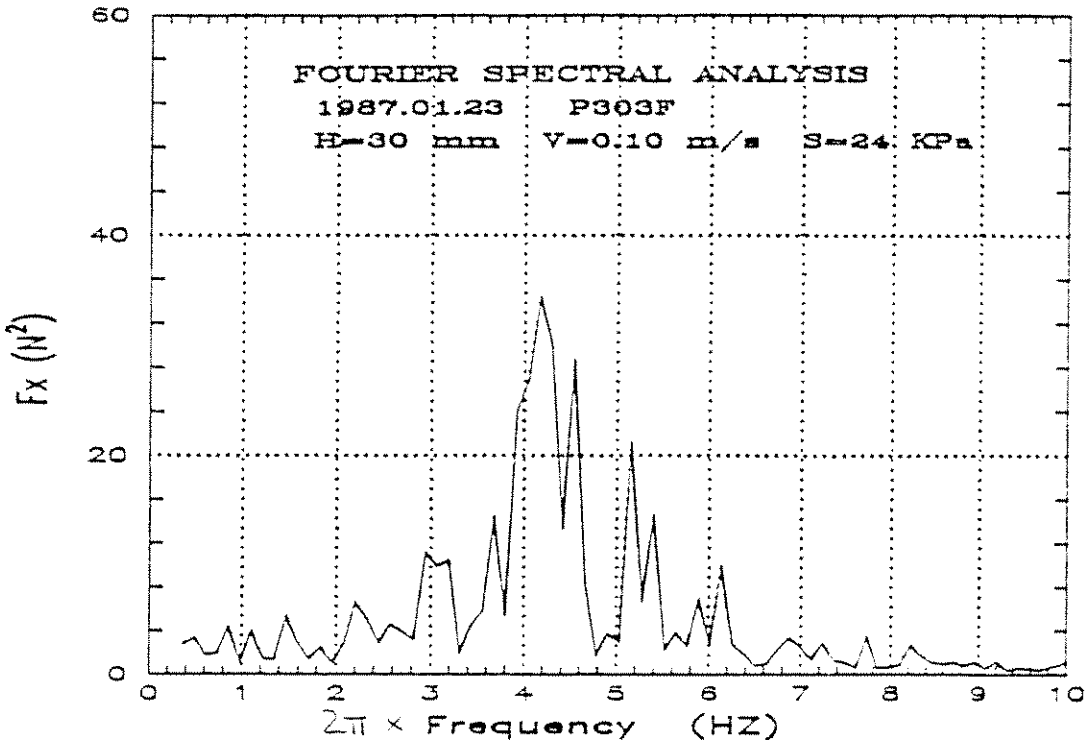

Figure 48. Frequency Power Spectrum for Fx, test P303F (fixed)

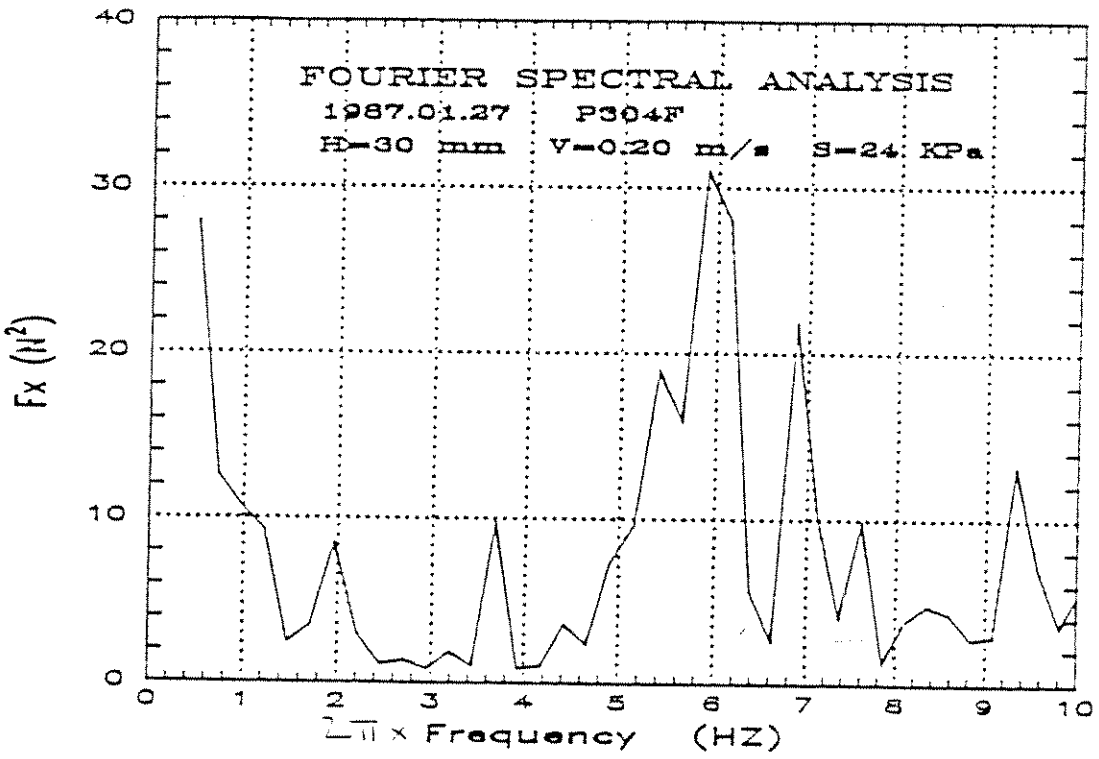

Figure 49. Frequency Power Spectrum for Fx, test P304F (fixed)